The Canadian Mineralogist
Vol. 38, pp. 915-936 (2000)

THE ROLE OF MAGMATIC PROCESSES IN THE FORMATION OF BANDED Li,F-ENRICHED GRANITES FROM THE ORLOVKA TANTALUM DEPOSIT, TRANSBAIKALIA, RUSSIA: MICROTHERMOMETRIC EVIDENCE

FELIX G. REYF[§]

Geological Institute (*GIN*), *Siberian Branch of the Russian Academy of Sciences, Sakhyanova 6a, Ulan-Ude, 670047, Russia*

REIMAR SELTMANN[§]

Department of Mineralogy, Natural History Museum, Cromwell Road, London SW7 5BD, U.K.

GEORGY P. ZARAISKY[§]

Institute of Experimental Mineralogy (*IEM*), *Russian Academy of Sciences, Chernogolovka, Moscow District, 142432, Russia*

Abstract

Quartz- and topaz-hosted melt, fluid, and mineral micro-inclusions have been studied to shed light on the origin of the massive and banded Li,F-enriched granites that host the Orlovka tantalum deposit, in Transbaikalia, Russia. Certain quartz and topaz grains, similar to most of the others in their morphology and structure, contain primary or secondary melt inclusions (or both), suggesting that these rocks are of magmatic origin. Their textural features are assumed to stem from different regimes of cooling of parental melts, as indicated by morphological peculiarities of rock-forming minerals. From thermometric and analytical studies of the melt and fluid inclusions, it follows that the Li,F-enriched granites were formed from melt that was enriched in F (~4 wt%) and H_2O (~6 wt%), contained CO_2 in addition to H_2O (mole fractions are ~0.08 and ~0.92, respectively), and had unusually low viscosity (~50 Pa•s at 660°C). The existence of quartz crystals that contain melt inclusions and columbite–tantalite microcrystals in the same growth-zones suggests that the melt became tantalite-saturated during early stages of crystallization at the top of the intrusion and late in the crystallization sequence at lower levels. With regard to results of model calculations, the uppermost position of the most Ta-rich melt in the pluton is considered to be caused by the removal of interstitial residual melt from deeper parts of the magmatic body and emplacement into a previously solidified crystalline carapace rather than by crystal settling.

Keywords: granite, tantalum, banded texture, melt inclusions, melt viscosity, Orlovka deposit, Transbaikalia, Russia.

Sommaire

Nous avons étudié des micro-inclusions de magma (verre), fluide et solides piégées dans le quartz et le topaze d'échantillons d'un granite massif ou rubanné enrichi en Li et F, situé au Transbaïkal, en Russie, afin de déterminer l'origine du gisement de tantale d'Orlovka, qui lui est associé. Certains grains de quartz et de topaze, semblables à la plupart des autres en morphologie et en structure, contiennent des inclusions vitreuses primaires ou secondaires (ou les deux), montrant que ces roches ont une origine magmatique. Leur développement textural serait dû au régime de refroidissement imposé au magma parent, comme en témoigne les particularités morphologiques des minéraux principaux de ces roches. A partir des études thermométriques et analytiques des inclusions vitreuses et fluides, les granites enrichis en Li et F se seraient formés à partir d'un magma enrichi en F (~4%, poids) et H_2O (~6%), contenant aussi du CO_2 [les fractions molaires dans la phase gazeuse étant ~0.08 (H_2O) et ~0.92 (CO_2)], et possédant une viscosité anormalement faible (~50 Pa•s à 660°C). L'existence de cristaux de quartz contenant à la fois des inclusions vitreuses et des microgermes de columbite–tantalite dans une même zone de croissance fait penser que le magma est devenu saturé en tantalite au cours des stades précoces de sa cristallisation au sommet de la chambre magmatique, et plus tardivement en profondeur. Selon nos calculs, la position apicale de la fraction magmatique la plus enrichie en Ta serait due à la migration du liquide résiduel interstitiel des parties profondes de la chambre vers le sommet, et sa mise en place dans une carapace cristalline déjà solidifiée, plutôt que par accumulation de cristaux vers le bas par gravité.

(Traduit par la Rédaction)

Mots-clés: granite, tantale, texture rubannée, inclusions vitreuses, viscosité, gisement d'Orlovka, Transbaïkal, Russie.

§ *E-mail addresses*: angin@burnet.ru, rs@nhm.ac.uk, zaraisky@iem.ac.ru

Introduction

Banded rocks observed in the endocontact parts of many small shallow bodies of granite consist of layers that differ strikingly in texture and composition. Conformity of the layers to a contact surface and crystal morphology indicating that the growth direction was inward to the magmatic body suggest a magmatic origin related to a temperature gradient (*e.g.*, White *et al*. 1981, Shannon *et al*. 1982, Carten *et al*. 1988, Webber *et al*. 1997, London 1998). On the other hand, 1) banded rocks are most typical of granite intrusions associated with hydrothermal ore deposits, 2) many layers are almost monomineralic or differ greatly from "normal" magmatic rocks in chemical composition, and 3) some layers are enriched in molybdenite or wolframite, beryl, fluorite and other minerals that rarely occur in unaltered igneous rocks (*e.g.*, Povilaitis 1961, 1990, Potap'ev 1971, Carten *et al*. 1988). These features of banded granites are not compatible with the regularities of equilibrium magmatic crystallization and, hence, lead one to suspect a significant role of a fluid phase in their formation, which is supported, in a special case, by Lowenstern & Sinclair (1996).

In this paper, we explore these issues by focussing on identification and examination of fluid and melt inclusions in the Orlovka topaz – Li mica – albite granite, in eastern Transbaikalia, both massive and banded, that will be hereafter referred to as Li–F granite. Banded rocks of similar composition are poorly studied, and the origin of topaz – lepidolite – albite granites (magmatic or metasomatic) is still controversial. In particular, some key examples of such rocks, formerly considered as albitized and greisenized biotite granite ("apogranite", after Beus *et al*. 1962), are considered at present to be of magmatic origin [*e.g.*, the Orlovka granite: Beus *et al*. (1962) and Koval (1975) *versus* Beskin *et al*. (1994), the Beauvoir granite: Aubert (1969) *versus* Raimbault *et al*. (1995), and the Yashan granite: Hu *et al*. (1984) and Xia & Liang (1985) *versus* Yin *et al*. (1995)]. In order to assess the role of magmatic processes in formation of the Orlovka Li–F granites and the associated Ta mineralization, we first established the paragenetic sequence of host minerals and their temporal relationships with minerals of columbite–tantalite group (hereafter, columbite–tantalite), and then proceeded to an investigation of the fluid and melt inclusions. Interpretation of the inclusion-derived data is made with emphasis on the peculiar properties of preserved melts and uncertainties inherent in the thermometric and analytical procedures used.

The present study is part of a more extensive investigation that will elucidate the mechanisms producing banded Li–F granite on the basis of petrographic, geochemical, isotopic, and experimental data. For preliminary data, see Zaraisky *et al*. (1997) and Seltmann *et al*. (1998).

Geology

The Orlovka tantalum deposit is located in Eastern Transbaikalia, Russia, 140 km southeast of Chita city, to the south of the Siberian craton, where Paleozoic (D–C_1?) metasedimentary rocks constitute the upper part of the Aginskaya microplate, which underwent widespread magmatism during the Early Mesozoic. In its northeastern part, the microplate was intruded by granite plutons, the largest of which, from gravimetric data, is 24 by 22 km in dimension at a depth of 3 km and is exposed at surface as three separate granitic bodies (cupolas): Khangilay (8 km^2) in the center, Spokoyny (0.06 km^2) in the east, and Orlovka (about 2 km^2) in the west (Potap'ev 1971, Beskin *et al*. 1994). For all these granites, K–Ar estimates of age vary from 136 to 74 Ma (Potap'ev 1971); a more recent Rb–Sr determination for the Orlovka granite yielded an age of 142 ± 3 Ma (Negrey *et al*. 1995).

At the surface and to a depth of about 450 m, the cupolas were found to be composed predominantly of porphyritic biotite granite. Other varieties of limited occurrence were considered to be either coeval igneous rocks or metasomatically altered biotite granite (Potap'ev 1971, Beskin *et al*. 1994). The Li–F granites occur only in the upper part of the Orlovka cupola and were originally described as albitized and greisenized biotite granite (Zalashkova 1969, Potap'ev 1971, Koval 1975; Fig. 1). More recently, additional field observations and detection of melt inclusions in topaz grains from these granites have served as a basis for the conclusion that the Li–F granites are magmatic in origin and form a separate sheet-like body emplaced between the underlying biotite granite and roof of the Orlovka cupola (Beskin *et al*. 1994).

Although there was disagreement among previous investigators on the role of magmatic and metasomatic processes in formation of the Li–F granite enclosing Ta mineralization, they were unanimous in distinguishing a zonation in the Orlovka granite cupola. As a result, the main features of the zoning shown in Figure 1 and expressed in terms of the metasomatic concept (Koval 1975) may be seen also in the map and cross-section that illustrate the structure of the sheet-like intrusion of Li–F granite (see Beskin *et al*. 1994). Outward from the central portion of the Orlovka cupola, which is composed of porphyritic biotite granite and two-mica granite, and above these in the cross-section (see Fig. 1), the Li–F granites become enriched in albite (29.5 to 44.6 vol.%), topaz (~0.1 to 2.8%), microlite (0–10 to 20–150 grams per tonne), and columbite–tantalite (60 to 150–800 grams per tonne). The Ta:Nb ratio in the latter increases along these lines from 0.57 to 2.36, Li-bearing muscovite gives way to lepidolite or zinnwaldite, and microcline turns into the variety "amazonite" (Zalashkova 1969, Koval 1975, Beskin *et al.* 1994). The granite of the uppermost zone is an orebody that has

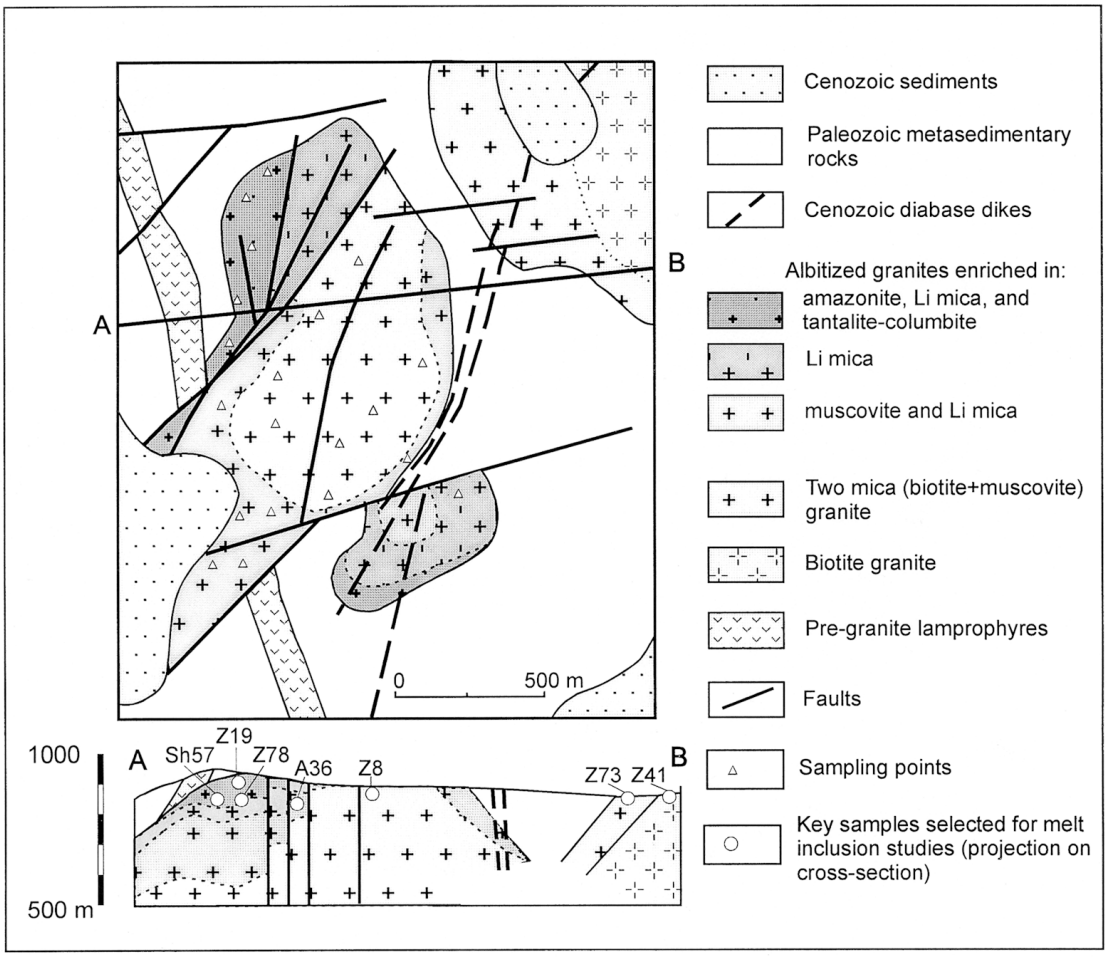

FIG. 1. Schematic geological map of the Orlovka cupola and cross-section derived from exploration- drilling data (modified after A.M. Grebennikov, V.I. Belykh *et al.*, unpubl. data) in terms of the apogranite concept (Koval 1975). The southwestern end of the Khangilai cupola is shown at the top right of the map.

been partly mined. It is remarkable that defenders of both the metasomatic and magmatic models for the Li–F granites assume enrichment of the upper zone in Ta, Nb, Li, Rb, F to be mainly caused by a redistribution of elements by postmagmatic hydrothermal solutions (Zalashkova 1969, Koval 1975, Beskin *et al*. 1994).

Banded rocks are confined to the upper, highly mineralized zone, where they form subhorizontal layers or flat lenses 0.1 to 1.5 m thick and up to several tens of meters in lateral extent within the massive Li–F granite. In addition, subordinate, steeply dipping dike-like bodies of the banded granite occur (Zaraisky *et al*. 1997). Alternating layers in these rocks all contain quartz, albite, microcline ("amazonite"), Li-enriched mica, and topaz. However, as a rule, only two, less commonly three, of these minerals are dominant in adjacent units, which permits recognition of layers (0.5 to 15 cm) composed predominantly of quartz–albite, or quartz–microcline ("amazonite"), or quartz–mica assemblages. In addition, some layers are relatively enriched in topaz or columbite–tantalite and beryl. Typically, quartz–albite layers are fine-grained (aplite-like), whereas quartz–mica and quartz–microcline layers are medium- to coarse-grained, and some have a pegmatitic texture.

Some layers, especially those that are microcline-rich, exhibit uniform orientation of elongate crystals which nucleated on the upper boundary of the layer and grew downward in the form of fan-like aggregates. Similar textures in silicic rocks are classified as "unidirectional solidification textures" (Shannon *et al*. 1982)

and are interpreted to reflect a thermal gradient during magmatic crystallization (Fenn 1977, Brandeis *et al.* 1984, Swanson & Fenn 1986). Nevertheless, banded rocks similar to those described above have been interpreted as products of profound hydrothermal alteration of the "quartz albitite" that forms xenoliths in the Orlovka Li–F granite and dikes in country rocks (Beskin *et al*. 1994).

Key samples

Although more than 30 samples were collected throughout the Orlovka cupola and adjacent part of the Khangilay cupola, only seven of these were chosen, after initial petrographic observation, for extensive study of melt and fluid inclusions (see Fig.1). Three of these represent porphyritic two-mica granite from the Khangilay cupola (Z41 and Z73) and the deep levels of the Orlovka cupola (Z8). Four samples represent the following varieties of the Li–F granites: massive, unbanded porphyritic granite, which is widespread at lower levels of the Li,F-enriched intrusion (A36), thin-banded granite enriched in columbite–tantalite and beryl as compared to other similar rocks (Z78), pegmatite–aplite rock that may be defined as a transitional type between the massive and thin-banded granites (Z19), and a 1.5-cm-thick pegmatite veinlet perpendicular to the thin-banded granite and, hence, representing one of the latest derivatives of the Li–F granites (Sh–57). The chemical compositions of these key samples are reported by Zaraisky *et al*. (1997) and reproduced below, and their mineralogical and textural features are described in the Appendix A; thus only the essential inferences related to the mineral sequence are presented below.

At least some of the muscovite in the two-mica granites crystallized simultaneously with quartz phenocrysts, whereas there is no evidence that biotite ever existed in the Li–F granites. These observations are inconsistent with the idea that the Li–F granite is a metasomatically altered biotite granite. In all Li–F granites, topaz occurs in both early- and late-stage mineral assemblages; columbite–tantalite occurs only in the late-stage mineral assemblage in granite from lower levels, but crystallized throughout the formation of granite in upper levels. Unidirectional growth of rock-forming minerals is typical only in upper-level granite.

Types of Inclusions, their Origin and Timing

Melt inclusions (MI) and fluid inclusions (FI) have been identified in rock-forming quartz and topaz in addition to the abundant crystalline inclusions described in Appendix A. Most of these MI and FI are confined to planes (healed microfractures) cutting the host minerals in various directions; hence they are secondary in origin with respect to the host. Melt and fluid inclusions classified as primary are confined to separate growth-zones (Fig. 2h) or are distributed randomly, singly or in small groups, without relation to healed microfractures and surfaces of thin sections. Primary inclusions also form isolated cloud-like clusters inside host crystals (grains) (Fig. 2g). Significant numbers of inclusions, however, are of ambiguous origin, because in many cases thin doubly-polished plates (0.3–0.4 mm) do not reveal the regularities in distribution of the inclusions throughout host crystals (grains).

Melt inclusions

Quartz- and topaz-hosted primary MI in the samples studied (Figs. 2a, b) are few in number and small in size (rarely in excess of 15 μm in diameter). Ribbon-like groups of the secondary MI, observed only in topaz, are rather scarce as well; some of these groups contain many tens of cogenetic inclusions, however. Few topaz grains contain both primary and secondary MI. A list of inclusions studied thermometrically and volumetrically is presented in Table 1, which shows that the melt inclusions are present in all key samples. Of course, some mineral grains in these samples do not contain MI. Nevertheless, there is no reason to assume that all grains devoid of MI are nonmagmatic in origin inasmuch as most of these grains are similar to the MI-containing counterparts in morphology, composition and distribution of mineral micro-inclusions.

Taking into account the nature of MI and the generation of host minerals, we assume the primary MI from the two-mica granites (Z8, Z41, Z73), the secondary MI from the massive Li–F granite (A36), and those from the Li–F veinlet pegmatite (Sh57) are relevant to the late-magmatic (near-solidus) stage of formation of the appropriate rocks. Both quartz- and topaz-hosted primary MI from the banded Li–F granites (Z19, Z78) are assumed to have formed during the main (subliquidus) stage of crystallization of these rocks.

At room temperature, both primary and secondary MI contain microcrystalline aggregates and spherical or deformed gas bubbles plus aqueous solutions, which typically occupy intercrystalline space and are indis-

TABLE 1. LIST OF MELT INCLUSIONS STUDIED FROM ORLOVKA

Sample	Label	Rock type	Host mineral	MI type	n[a]	T[b], °C
Z73	1-8	Biotite granite	Qtz, mtrx	Prim.	5	650; 700
Z8	1-9	Biotite granite	Qtz, mtrx	Prim.	22	650; 750; 800
Z19	1-5	Aplite layer with Amz megacrysts	Toz,mtrx	Prim.	2	650; 700
Z19	2-4	Aplite layer with Qtz megacrysts	Toz	Prim.	4	700
Z19	2-3	Pegmatoid layer	Qtz, mtrx	Prim.[c]	2	700
Z78	1-10	Quartz-enriched layer	Qtz	Prim.[c]	2	650; 700
Z78	2-1	Quartz-enriched layer	Qtz	Prim.[c]	6	700
A36	1-7	Massive Toz-bearing granite	Toz	Sec.[c]	154	650; 700; 800
A36	2-6	Massive Toz-bearing granite	Toz	Sec.[c]	73	750
Sh57	1-6	Pegmatite veinlet	Toz	Sec.	17	650; 750; 800
Sh57	2-5	Pegmatite veinlet	Toz	Sec.	14	750

[a] Number of MI studied thermometrically.
[b] Temperatures at which the melt inclusions were heated under confining argon pressure of 5 kbar; underlined digit signifies the run temperature after which quenched inclusion became homogeneous (glass without fluid bubble).
[c] Cogenetic magmatic fluid inclusions (MFI) are present.

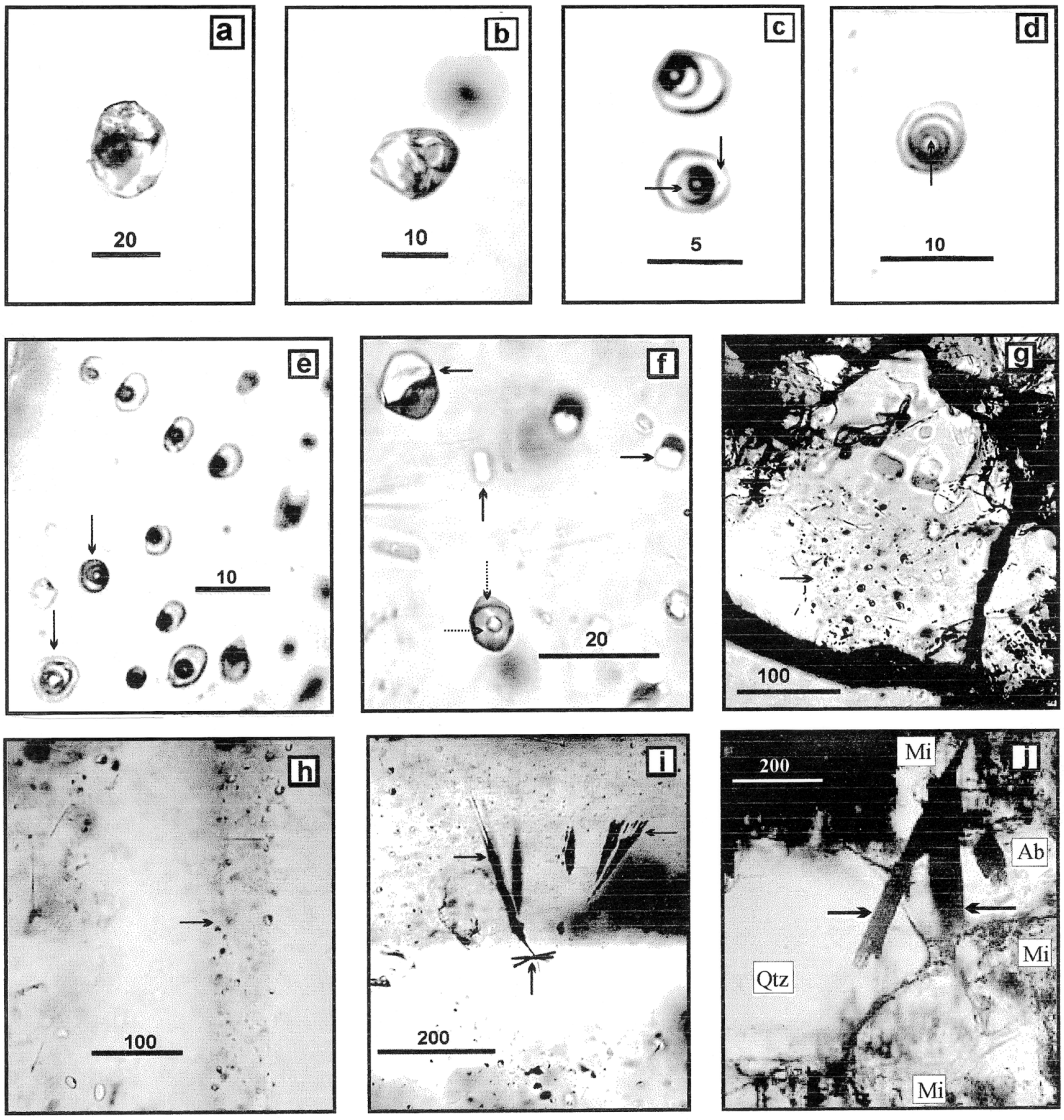

FIG. 2. Digital micrographs showing melt and fluid inclusions and structural peculiarities of some rock-forming minerals from the Li–F granites: (a, b) Unheated primary melt inclusions in topaz and quartz, respectively. (c) Two images of the same melt inclusion quenched after 1.5 h of exposure at 642°C (upper image) and subsequent 2 h of exposure at 660°C (lower image). Observed migration of the fluid bubble, heterogeneous at room temperature (horizontal arrow), in melt, now glassy (vertical arrow), has taken 90 minutes at 660°C. (d) Topaz-hosted inclusion formed *via* entrapment of two immiscible phases, silicate melt and CO_2-rich fluid, and quenched after 20 h of exposure at 700°C, 5 kbar confining argon pressure. Concentric envelopes surrounding the gas bubble (arrow) are: liquid CO_2, aqueous solution, and glass. (e) Healed microfracture in topaz comprising inclusions of silicate melt and exsolved CO_2-rich fluid (arrows) quenched after 20 h exposure at 700°C, 5 kbar confining pressure. The combined inclusion shown in the previous micrograph lies in this microfracture. (f) Quartz-hosted, unheated primary MFI, containing aqueous solution (vertical dotted arrow) and liquid-gaseous CO_2 (horizontal dotted arrow), is confined to the growth zone enriched in topaz micro-inclusions (vertical solid arrow), generally combined with MFI (horizontal solid arrows). (g) Zoned groundmass quartz whose core (arrow), by contrast to rim, is filled with MFI and topaz microcrystals. (h) Intermittent growth-zones of quartz megacryst, enriched in MFI, MI, and topaz micro-inclusions (arrow) and free of them. (i) Change in habit of tantalite from acicular (vertical arrow) to dendritic (horizontal arrows) as growth zone of quartz almost free of inclusions gives way to that filled with MFI, MI, and topaz micro-inclusions. (j) Columnar crystals of columbite–tantalite (horizontal arrows) whose opposite terminations are hosted by different mineral grains in the aplitic Li–F granite. Length of scale bars is given in μm. The micrographs are obtained using the digital camera Kodak DC 210.

TABLE 2. EPMA DATA ON COMPOSITION (IN WT %) OF SOME CRYSTALLINE PHASES FORMING TOPAZ-HOSTED MELT INCLUSIONS AND MINERAL MICRO-INCLUSIONS IN QUARTZ FROM THE TWO-MICA AND Li-F GRANITES

No.	Sample	Mineral	SiO_2	TiO_2	Al_2O_3	FeO	MnO	MgO	CaO	Na_2O	K_2O	F	Cl	P_2O_5	Total minus O≡F
Crystalline phases forming melt inclusions															
1	Z78	Muscovite	47.96	<0.05	33.52	0.25	0.30	<0.04	0.22	0.22	9.89	1.41	<0.02	n.a.	93.18
2	- " -	Fluorite[a] ?	13.6	0.06	2.29	0.16	0.05	<0.03	32.73	0.15	0.04	30.87	<0.03	n.a.	79.95
3	- " -	Quartz	100.06	<0.05	0.20	<0.10	<0.03	<0.04	<0.04	<0.05	<0.02	<0.33	<0.03	n.a.	100.26
4	A36	Quartz	99.49	<0.05	0.47	<0.07	<0.03	<0.04	<0.05	<0.09	0.03	<0.48	<0.05	n.a.	99.99
5	- " -	Microcline	63.11	n.a.	22.89	0.24	<0.03	<0.04	0.23	1.57	12.44	1.55	<0.05	n.a.	101.38
Mineral micro-inclusions															
6	Z73	Biotite	36.52	3.13	16.17	22.03	0.55	5.45	0.17	0.09	9.69	1.24	0.08	<0.05	94.60
7	Z41	Muscovite	45.22	<0.04	36.86	1.20	0.06	<0.06	<0.03	0.66	10.46	0.55	0.01	<0.05	94.79
8	Z73	Muscovite	44.12	0.09	34.90	0.35	0.03	<0.06	0.24	0.30	10.49	0.49	0.02	0.05	90.87
9	Z78	Zinnwaldite[b] ?	43.51	n.a.	21.27	14.86	0.93	<0.07	<0.02	0.08	9.91	4.81	0.02	n.a.	93.37
10	- " -	Zinnwaldite[b] ?	43.04	n.a.	22.30	13.91	1.35	<0.07	<0.02	0.09	10.10	5.23	<0.02	n.a.	93.82
11	Z78	Albite	68.39	n.a.	19.44	n.a.	n.a.	n.a.	0.05	11.69	0.10	n.a.	n.a.	n.a.	99.67
12	Z73	Fluorapatite	0.44	<0.04	<0.08	0.12	0.26	<0.07	55.44	0.22	0.05	4.88	0.02	41.10	100.48
13	Z78	Topaz	32.17	<0.06	54.05	<0.10	<0.05	<0.10	<0.02	<0.05	<0.02	17.70	n.a.	n.a.	96.47
14	- " -	Topaz	31.56	<0.04	54.66	<0.07	<0.04	<0.07	<0.02	<0.04	<0.01	15.77	n.a.	n.a.	95.35
15	- " -	Topaz	31.75	<0.04	55.10	<0.07	<0.03	<0.07	<0.02	<0.04	<0.01	16.33	n.a.	n.a.	96.31
16	Z41	Fluorite[c]	0.21	0.06	<0.04	0.09	n.a.	<0.04	53.93	0.06	0.08	47.21	0.02	n.a.	101.66
17	Z73	Fluorite[c]	0.14	<0.05	<0.04	0.08	n.a.	<0.04	52.93	<0.05	0.47	46.52	0.02	n.a.	100.16
18	Z19	Fluorite[c]	0.13	n.a.	<0.04	0.09	0.07	<0.04	50.55	0.08	<0.02	48.76	0.02	<0.02	99.70

n.a., not analyzed.
[a] Excess of Si and Al is assumed to be resulted from excitement of adjacent daughter quartz and host topaz.
[b] Expected H_2O and Li_2O contents are ~2.8 and 3.7 wt %, respectively.
[c] Composition is presented in wt % elements rather than their oxides.

cernible visually (Figs. 2a, b). Upon heating, however, the gas bubble decreases in size and dissolves into the solution (it reappears during cooling). Owing to the scarcity of large MI, only a few crystalline phases were analyzed within two topaz-hosted MI using electron-probe micro-analysis (EPMA). These phases are quartz (No. 3 and 4 in Table 2), K-feldspar (No. 5), muscovite (No. 1), and fluorite-like fine particles (No. 2). Sodium-rich phases are not detected in these inclusions. They are believed to have been either ground off or, conversely, covered by other minerals. It must be noted that the dominant daughter phases quartz and muscovite were identified in topaz-hosted MI previously in the Volyn' pegmatites (Lemmlein *et al.* 1962) and in the Akchatau ongonite-like dikes (Reyf *et al.* 1989). These minerals (±albite, microcline) and, to a lesser extent, natrosilite are also typical of quartz-hosted crystallized MI from various topaz-free granites (*e.g.*, Reyf 1973, 1990, 1997, Stelmachonok & Kanakin 1992). The minerals present in quartz-hosted MI from the Orlovka granites are not yet identified owing to their small size.

As a rule, primary MI in topaz are not associated with cogenetic fluid inclusions, whereas some healed microfractures in topaz from the massive and banded granites and pegmatite veinlet contain cogenetic MI and FI (Fig. 2e). All quartz-hosted MI were found within the growth-zones which, as compared to adjacent ones, are highly enriched in the cogenetic FI and topaz microcrystals. Certain MI-containing growth-zones are enriched not only in topaz, but also in columbite–tantalite microcrystals (Figs. 2i, 3).

Fluid inclusions

Taking into account that some growth-zones in quartz grains and healed microfractures in topaz grains contain cogenetic MI and FI, the latter are considered to be representative samples of the fluid exsolved from the melt; thus they will hereafter be referred to as "magmatic fluid inclusions" (MFI). The great majority of the MFI are small in size (<10 μm) and similar in phase composition. At room temperature, both primary and secondary MFI contain liquid and gaseous CO_2 in addition to an aqueous solution, which forms a barely visible film in most of the inclusions (10 to 20% by volume) or occupies up to 85 vol. % in certain of the MFI populations. All the MFI in separate quartz grains, even those that are zoned and large in size, are visually indistinguishable from each other relative to the volume portion of aqueous solution. However, the latter varies

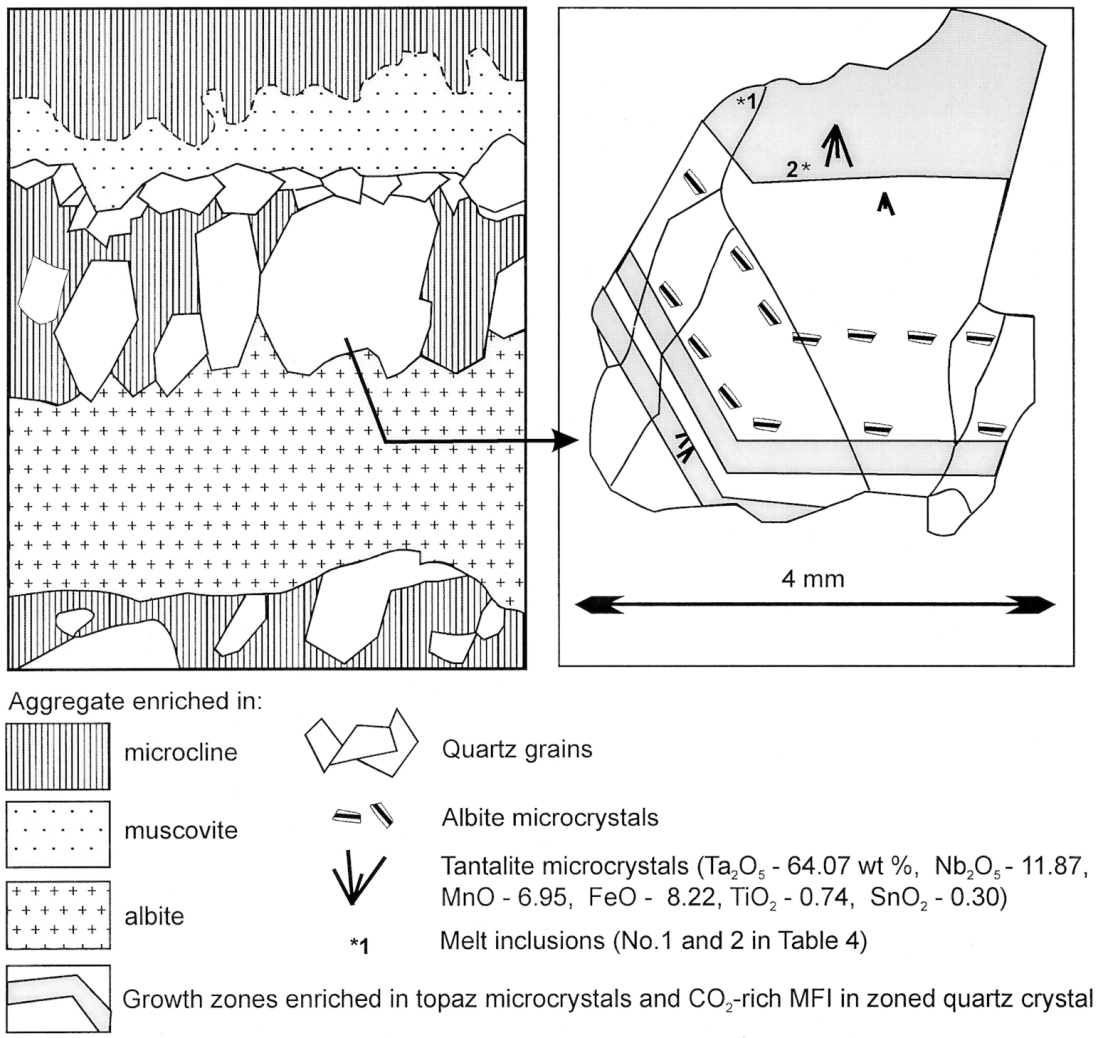

FIG. 3. Schematic sketch of the thin-banded Li–F granite (sample Z78) and magnified image of a zoned quartz crystal from a medium-grained layer.

distinctly from grain to grain in the fine-grained Li–F granite (Z19). Inasmuch as the most H_2O-enriched MFI occur, along with MI, within the healed microfractures, the H_2O content of the exsolved fluid is likely to increase as degassing of the magma progresses.

Within growth-zones enriched in crystalline microinclusions, the MFI are usually associated with topaz (Fig. 2f), but rarely with albite. In healed microfractures containing MI and MFI, some inclusions of both types are integrated by accident, resulting in formation of "combined" inclusions. As a rule, the latter are not visually distinguishable among unheated MI; they become discernible after heating at 640–660°C and quenching because the glass in these inclusions contains enlarged three-phase bubbles [aqueous solution, liquid CO_2, and gaseous CO_2 (Fig. 2d)].

Neither the CO_2-free inclusions nor those containing daughter crystals were observed among the MFI. As to the secondary FI not associated with MI, most of them also contain liquid CO_2, whereas two-phase aqueous secondary inclusions are scarce.

RESULTS OF MICROTHERMOMETRY

The goals of the thermometric examination of MI were: (1) to determine a homogenization temperature

for the inclusion fluid constituent (T_{h-fl}), which makes it possible to calculate an H_2O content of MI (C_{w-mi}) based on the procedure described by Naumov (1979) and Reyf (1990), (2) to measure a temperature at which MI becomes homogeneous (T_h) and obtain glassy inclusions suitable for electron-microprobe analysis, and (3) to estimate salinity and CO_2 content of FI and MI fluid constituents. The instrumentation and techniques used in this study are described in the Appendix B.

Melt properties

The fluid constituents of all MI studied that are heterogeneous at room temperature homogenize to liquid at $210 < T_{h-fl} < 290$°C. This range corresponds to a bulk fluid density of 0.79 to 0.90 g•cm^{-3}, assuming a salinity of about 5 wt% NaCl equivalent (see Table 3, label *e*). Using these data and measurements of volumes of the gas bubble and MI, the H_2O content is calculated for a series of MI from all key samples (Fig. 4). The calculated values suggest that the late-stage melt in the Khangilay cupola contained about 4.5–5 wt% H_2O, whereas H_2O content of the main-stage melt of Li–F granites was close to 6 wt% and increased to ~12% at the final stage of crystallization (Fig. 4). The value of 6 wt% H_2O is in agreement with experimentally determined solubilities of H_2O in F-enriched granite melts at 1 to 2 kbar and T ≤ 800°C (Kovalenko 1979, Webster 1990, Holtz *et al*. 1993). The highest estimates obtained in this study (~12 wt% H_2O), are consistent with certain H_2O solubilities reported [up to 10.9 wt% H_2O at 1 kbar, 750°C, 3.4 wt% F in melt: Kovalenko (1979); up to 11.5 wt% H_2O at 2 kbar, 650°C, 0.9 wt% F in melt: London *et al.* (1988)], but they are ~1.5 times greater than experimental results by Holtz *et al.* (1993). Because of the small size of the MI, we were unable to check these estimations for accuracy using secondary-ion mass spectrometry (SIMS) or Fourier transform infrared spectroscopy (FTIRS). However, data reported by Thomas & Klemm (1997) confirm that our procedure yields results that are commensurate with those obtained *via* EPMA and SIMS.

Upon heating above 400°C, almost all MI in excess of ~5 μm in diameter decrepitate, that is, turn irreversibly dark because of leakage of their fluid constituent through microcracks that appear owing to increasing internal fluid pressure which, as follows from the Burnham model, may far exceed the pressure at the time of trapping (Burnham 1979, Student & Bodnar 1996). In accordance with determined salinity of the fluid (~5 wt% NaCl equiv.) and density (0.79 to 0.90 g•cm^{-3}), the calculated internal pressure in our MI attains 2.5–4.7 kbar at 500°C, prior to the beginning of melting of the crystalline phases. The latter begin to melt at ≤600°C, and only two phases, melt and gas bubble, are discernible under a microscope in inclusions that remain undecrepitated at 620°C. After chilling, these inclusions contain glass and a fluid bubble, gaseous in decrepitated MI and gas–liquid in undecrepitated ones (Fig. 2c).

Because heating at atmospheric pressure fails to prevent the decrepitation of relatively large MI, most of them were heated under a confining argon pressure of 5 kbar during 8 to 20 h at a preselected temperature. This procedure (Appendix B) precludes observations of the inclusions during heating, thus their phase assemblage at run conditions can only be determined if the inclusion is "frozen" *via* quenching, much as happens when chilling homogenized MI from "normal" granites. For example, even small (4 μm) MI hosted by a groundmass quartz grain from the Khangilay biotite granite (sample Z73) displayed incomplete melting of the crystalline phases after 8 h of heating under 5 kbar confining pressure at 650°C, whereas all these inclusions, as well as those 9 μm in diameter, became totally homogeneous (glassy) after heating for 20 h at 700°C ($650° < T_h \leq 700$°C).

In contrast, both quartz-hosted and topaz-hosted MI from the Orlovka granites, quenched after sequential experiments performed at 650°C (8 h), 700°C (20 h),

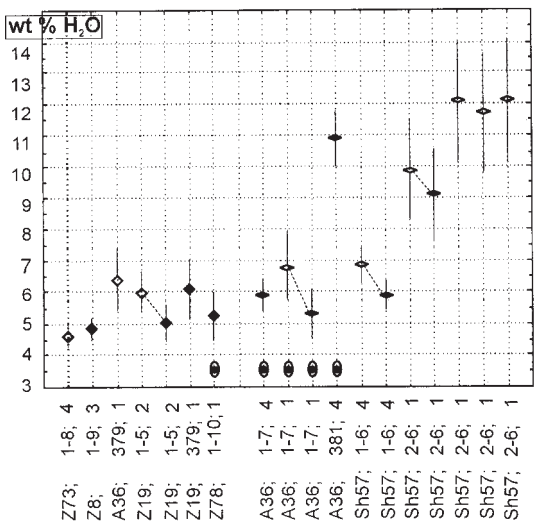

FIG. 4. H_2O content of the melt inclusions computed from microthermometry and volumetry that were conducted prior to and after heating up to 700°C at argon pressure of 5 kbar and following chilling (open and filled symbols, respectively). Results obtained using both procedures for the same MI are connected with dashed line. Normal and flattened rhombus are primary and secondary melt inclusions, respectively. MI associated with MFI are marked with symbol above abscissa. Figures following a sample number are the label of MI group and, next, number of inclusions measured. Bars are ± one standard deviation for the single measurement or ± one standard error for the mean of several measurements.

750°C (8 h), and even at 800°C (14 h), contain a fluid bubble in glass. This finding suggests that a homogeneous state of the inclusions was never attained at these run conditions. Such a scenario, however, seems to be unrealistic for the following reasons. On the one hand, the measured volume portion of fluid constituents in every group of cogenetic MI not associated with fluid inclusions is relatively uniform (relative standard deviation ≤25%), suggesting that the fluid was exsolved from trapped melt rather than the result of simultaneous trapping of melt and a coexisting immiscible fluid phase. On the other hand, low-temperature examination of glass-hosted fluid bubbles in the relatively large (10 μm) MI from sample Sh57 shows that the fluid is poor in carbon dioxide and contains ~4.8 wt % NaCl equivalent (see Table 3, label *e*). Such a fluid is highly soluble in any melt, and hence the H_2O mass in a glass-hosted fluid bubble must be significantly lower than in the fluid constituent of this MI prior to heating. These estimations, however, differ insignificantly, although a slight deficit in H_2O content of the quenched glassy MI is regular, suggesting that about 1 wt% H_2O remains dissolved in glass after quenching (symbols tied with dashed line in Fig. 4).

The above data allow us to assume that, at least in some heating experiments, the fluid was entirely dissolved in the MI at run conditions and later exsolved during chilling. From our experience, similar behavior is typical for MI from granites containing magmatic topaz or fluorite and is thought to be caused by the reduced viscosity of F-enriched melts (Reyf *et al*. 1989, Negrey *et al*. 1989).

Evidence for the low viscosity of the inclusion melt

A key piece of evidence for the low viscosity of the entrapped melt is the fact that the gas bubbles in several topaz-hosted MI from sample A36 changed their positions at 640°–660°C in a time as short as 1 to 1.5 h. This attests to abnormally low viscosities of the melt, which is quite unusual for MI from "normal" granites. This bubble motion is subtle at any moment, but it is readily detected through sketching or taking serial microphotographs at regular intervals. Such micrographs (Fig. 2c) made it possible to measure a horizontal projection of the pathway traversed by the bubble in 90 minutes (by ignoring its vertical component), and to calculate the velocity (1×10^{-10} m•s^{-1}). In principle, just as the buoyancy of gas bubbles may induce their motion, which is not necessarily vertical in a closed volume, so also can melt convection, induced by a temperature gradient (D*T*) at inclusion walls. Assuming that D*T* cannot exceed 1°C in a 20-mm inclusion and using "reasonable" values of the thermal conductivity, $\lambda = 0.963$ J•m^{-1}•s^{-1} • K^{-1}, heat capacity, $C_p = 1340$ J•kg^{-1}•K^{-1}, melt density $r_m = 2200$ kg•m^{-3}, melt thermal expansion $\alpha = 5 \times 10^{-5}$ K^{-1}, and melt dynamic viscosity $\eta = 10^4$ to 10 Pa•s (Sharapov & Golubev 1976, Jaupart & Brandeis 1986), we found the Rayleigh number *Ra* to be $\leq 2.7 \times 10^{-9}$ and the Reynolds number *Re* to be $\leq 3.7 \times 10^{-9}$.

Perceptible convection in a closed spherical volume is known to begin at $Ra \geq 10^3$ (Kutateladze 1990) and, with accepted parameters, would be possible only if the inclusion were ≥0.145 m in diameter. This means that the bubble motion in our case was governed by gravity rather than by melt convection, and hence, the melt viscosity may be estimated using a Stokes-like formula (bubble as a solid sphere):

$$V = \frac{2\, g \bullet \Delta\rho \bullet r^2}{9 \bullet \eta} \qquad (1)$$

or, more precisely, a Hadamard–Rybczynski formula (vapor bubble with internal circulation):

$$V = 2\,\frac{g \bullet \Delta\rho \bullet r^2}{\eta'} \bullet \frac{1 + \eta'' / \eta'}{6 + 9 \bullet \eta'' / \eta'} \approx \frac{g \bullet \Delta\rho \bullet r^2}{3 \bullet \eta'} \qquad (2)$$

where *V* is velocity (10^{-10} m•s^{-1} in our case), *g* is gravity (9.8 m•s^{-2}), $\Delta\rho$ is the difference between melt and fluid densities (2200–600 = 1600 kg•m^{-3}), *r* is bubble radius (9.5×10^{-7} m), η' and η'' are melt and fluid viscosities, respectively ($\eta'' = 6 \times 10^{-5}$ Pa•s).

The calculated value of the viscosity of entrapped melt at 660°C and ~5.9 wt% H_2O (Table 4, Fig. 4) is 47 Pa•s (31 Pa•s using the Stokes formula). This estimation seems unreasonable because it is about three orders of magnitude lower than the experimentally determined viscosities of granitic melts with similar H_2O contents at the same temperature (*e.g.*, Persikov 1984, Dingwell *et al*. 1996). Also, from melt-inclusion data obtained using the "quenching" method of Thomas (1994), it follows that viscosities of preserved F-poor granitic melts range from 10^6 to10^5 Pa•s at 800 °C. At the same time, the determined viscosities of the F- and P-rich pegmatite-forming melts are found to be as low as 10^3 to 10^1 Pa•s at 800 °C (Thomas *et al.* 1996), and our estimation falls within this interval. Nevertheless, the inclusions under discussion may well contain aluminofluoride "melt", whose coexistence with F-rich granitic melt is shown experimentally to be possible (Gljuk & Anfilogov 1975, Kovalenko 1979). This problem can be only solved by the determination of the composition of glassy MI and will be considered below.

In any case, owing to the low viscosity of the included melt, the homogenization temperature could not be determined. Therefore, a temperature of formation (T_f) of the Orlovka granites was estimated from the following data. On the one hand, the easily discernible fluid bubble was observed in several undecrepitated secondary topaz-hosted MI (sample A36) at 660°C during examination in a heating stage. On the other hand, a solidus temperature close to 700°C is determined for the Khangilay biotite granite (see above), which does not contain topaz and is poorer in H_2O than the Orlovka

TABLE 3. RESULTS OF THE LOW-TEMPERATURE EXAMINATIONS OF THE INCLUSION AND CALCULATED FLUID COMPOSITIONS AS IF IT WAS IN THE TERNARY SYSTEM H_2O-CO_2-NaCl

Sample:	Z78	Z78	Z19	Sh57	Sh57	A36	A36
Inclusion type:	MFI	MFI	MFI	MI	MFI	MFI	MFI
Labels corresponding to those in Fig. 5:	*a*	*b*	*d*	*e'*	*f*	*g*	*h*
Melting temperature, °C:							
solid CO_2	-57.4	-57.4	n.m.	n.o.	-56.9	-57.2	-57.2
ice	n.o.	n.o.	n.m.	-3.6	n.o.	n.o.	n.o.
clathrate, beginning	n.o.	n.o.	n.o.	0.5	n.o.	n.o.	n.o.
clathrate, final	8.1	8.1	8.1[a]	4.0	8.1[a]	8.1[a]	8.1[a]
CO_2 phases homogenization temperature, °C[b]	24.4	24.4	26.0[b]	n.o.	22.5	23.4	21.6
CO_2 phase volume fraction[c]	0.9	0.8	0.29	0.17	0.15	0.27	0.16
Fluid composition, mole fractions:							
H_2O	0.274	0.456	0.884	0.955	0.923	0.879	0.956
CO_2	0.722	0.538	0.106	0.030	0.066	0.111	0.033
NaCl	0.003	0.006	0.010	0.015	0.011	0.010	0.011
Aqueous solution salinity, wt % NaCl equivalent	3.8	3.8	3.8	4.8	3.8	3.8	3.8

n.m., not measured; n.o., not observed.
[a] not measured, accepted by analogy with MFI from Z78.
[b] homogenization into liquid in the all listed MFI, except for that labeled *h*.
[c] mean of 3 to 4 measurements for each MFI group.

granite (Fig. 4). The solidus of the Li,F-enriched magma is therefore assumed to be in the interval $660° < T < 700°C$.

Properties of the fluid phase

In order to determine the composition of volatiles, both those dissolved in the melt and those exsolved from it during crystallization of the Li–F granite, the fluid bubble in one of the glassy MI and certain MFI from some key samples was studied using a low-temperature technique. The fluid composition was computed using the programs CLATCOM (Yerokhin 1993) and FLINCOR (Brown 1989), with the assumption that the fluid is in the ternary system H_2O–CO_2–NaCl (Table 3). Although the fluid in our case is expected to contain F in addition to Cl, it is unlikely that the use of the simplified system for calculations can introduce large errors in the results because total salinity of the liquid phase is low (no visible salt crystals appear at negative temperatures).

Assuming the calculated bulk salinity of the inclusion to be negligible, the data may be generalized using the diagram constructed by Ryabchikov (1975) for the system granite–H_2O–CO_2. This diagram displays a relationship between two volatile components, H_2O and CO_2, in coexisting melt and exsolved fluid (dashed and solid curves, respectively, in Fig. 5A) as temperature decreases at constant pressure (2 kbar). The diagram cannot be applied completely to the Li–F granite inasmuch as addition of F in the model system would shift the curves toward lower temperatures. Nevertheless, we can interpret our data qualitatively.

The square labels *a, b, d, e* in Figure 5 are in accord with those in Table 3 and signify a composition of the quartz-hosted MFI associated with the primary MI, whereas round labels *f, g, h* in Figure 5B relate to the MFI confined, along with the secondary MI, to healed microfractures in topaz. If the cooling pathway of a hypothetical melt is presented by the vector *c* in Figure 5A, a fluid phase would appear in the model system at point *a'*, with $X(CO_2)$ in the coexisting melt and fluid corresponding to positions of points *a'* and *a*. With a temperature decrease, the mole fraction of CO_2 in the crystallizing melt would evolve from *a'* through *b'* and *e'* to *d'*, whereas $X(CO_2)$ in the exsolved fluid would change from *a* through *b* and *e* to *d*.

Within the framework of the model system, one can infer that if the most CO_2-rich of the MFI studied corresponds in composition to point *a*, then the volatile composition associated with the Orlovka parental magma is specified by point *a'* [$X(H_2O) = 0.92$, $X(CO_2) = 0.08$]. On the other hand, the fluid constituents of the secondary topaz-hosted MI from the pegmatite veinlet, which are assumed to be the latest derivatives of the Li–F magma, correspond to point *e'* [$X(H_2O) = 0.97$, $X(CO_2) = 0.03$]. This finding suggests that the pegmatite-forming melt was a product of advanced degassing of the

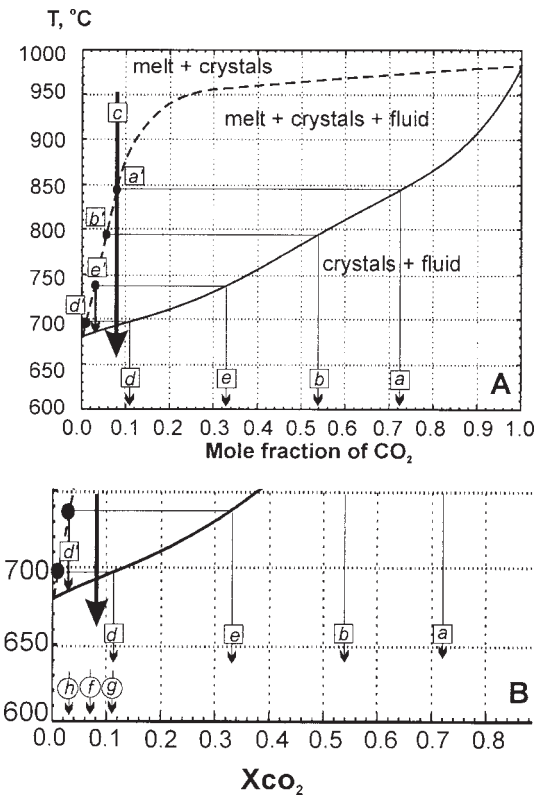

FIG. 5. Relationship between volatile components in coexisting melt and exsolved fluid in the system granite–H_2O–CO_2 at 2 kbar by Ryabchikov (1975). Lower diagram is a magnified part of the upper one. Labeled arrows show compositions of the inclusions studied; labels correspond to those in Table 3 (see text for explanation).

hypothetical parental melt. Also, all MFI studied associated with the secondary MI are strongly depleted in CO_2 (points *f, g, h* in Fig. 5B), as if microfractures were healed by a residual melt.

From the above, it may be deduced that the observed variation in the MFI compositions reflects the compositional evolution of the fluid exsolved from a CO_2-bearing hydrous magma. If so, the predominance of the most CO_2-rich MFI in quartz from the thin-banded granites, which is similar to that of sample Z78, suggests that these rocks were formed very early during degassing of the Li,F-enriched magma. Unfortunately, a similar line of reasoning cannot be applied to the massive Li–F granite, which is devoid of primary MFI.

Composition of the Melt Inclusions

The results of electron-microprobe analysis of the glass in the remelted MI from quartz and topaz vary widely from inclusion to inclusion and, in some cases, from point to point within single inclusions: SiO_2 ranges from 48 to 72 wt %, Al_2O_3 from 12 to 35%, K_2O from 1 to 6%, Na_2O from <0.06 to 6%, and F from 1 to 7%. In principle, the scatter in analytical data may reflect:

1) either the real diversity in composition of trapped melts, resulting either from geochemical evolution of a liquid phase in crystallizing magma, or from coexistence of immiscible liquids, or from enrichment of melt layer adjacent to dissimilar growing minerals in different incompatible elements,

2) or the difference in composition of analyzed *glasses* that may occur, even though all MI contained the same melt, if these MI were heated at different temperatures or some MI were too large for crystalline phases to melt completely or for the melt to equilibrate with the host mineral at given temperature and duration of heating,

3) or the failure to obtain representative compositions owing to some peculiarities of the analytical procedure or of the object that was studied.

Although none of these possibilities can be excluded *a priori*, certain of these may be discarded in specific cases. In particular, in view of the evidence for the very low viscosity of the trapped melt, it is unlikely that the causes listed above in the points (1) and (2) may be responsible for the scatter in the analytical data related to compositions of different parts of a single glassy MI or to compositions of several secondary MI, uniform in size, confined to one healed microfracture and remelted simultaneously at a temperature somewhat in excess of the expected T_h (see description below).

The above reasons allow us to infer that the most probable causes of the scatter under discussion are: (a) instability of a hydrous glass under the electron beam, resulting in migration of Na, K, and F during analysis, and (b) small size of the melt inclusions studied, which makes possible partial excitement of the host mineral. To minimize these factors, it is usual to use a defocused electron beam (spot size ≥15 μm) and to select only large inclusions (≥40 μm) for analysis. However, MI at least 15 μm in diameter are scarce in the Orlovka granites and, in addition, fluid bubbles in remelted MI make it difficult to prepare glassy areas that are more than 6 by 8 μm in size for analysis with a defocused electron beam.

As a result, the relative intensity of Na and K spectral lines ($J \approx$ wt% Na_2O or K_2O) registered at one "point" at equal intervals drops quickly, and the averaged value of J is always lower than the first measurement (Fig. 6). In the cases studied (15 analyses with count times of 25 s divided into five equal intervals), the dependence of J on time τ is well described by the equation $J = a \cdot (a + \tau)^b$. This allows the calculation of J value at "zeroth" time, which is believed to correspond most closely to the true concentration (Fig. 6). In Table 4, the analytical results adjusted in such a manner are marked "c".

Possible distortion of the analytical results due to excitement of a host mineral may be considered using compositions of topaz-hosted melt inclusions obtained using scanning electron microscopy with energy-dispersion spectrometry (SEM–EDS). At first glance, the SEM–EDS data shown in Figure 7 indicate that the central part of the glassy MI (point 1) differs from the outer one (point 2) in elevated Si concentration and reduced Al concentration, as if melt adjacent to the inclusion walls was contaminated by topaz, for example, because of overheating above the trapping temperature. In this case, however, the run temperature (750°C) was only 50°C in excess of the expected temperature of homogenization; a lack of strong overheating is corroborated by the observation that the inclusion dimensions prior to and after heating are identical. Moreover, compositions recorded at points 3 and 4 (Fig. 7) differ from each other as if the host mineral in the vicinity of the MI was contaminated by the inclusion glass, which is considered impossible. At the same time, all these discrepancies can be explained on the assumption that the electron beam, at point 2 for example, excites not only the glass but the adjacent topaz as well.

Additional evidence in favor of such assumption comes from the EPMA data of five cogenetic MI confined to a single healed microfracture in topaz from the sample Sh57 (Fig. 8). Melt inclusions 2 to 5 were analyzed at 1–3 points each at a single level, whereas MI–1 was ground (polished) three times, *i.e.*, became reduced in thickness, and analyzed at each level at a central point. Although data points in Figure 8 form two groups, as if two melts, a SiO_2-rich and a SiO_2-poor were trapped by different inclusions, it seems evident that the MI–1 data point shifts to the right owing to partial excitement of host topaz when the thickness of the inclusion glass becomes too small. In the light of this finding, the MI–2 and MI–4 are thought to have been ground excessively, resulting in excitement of the underlying material of the host.

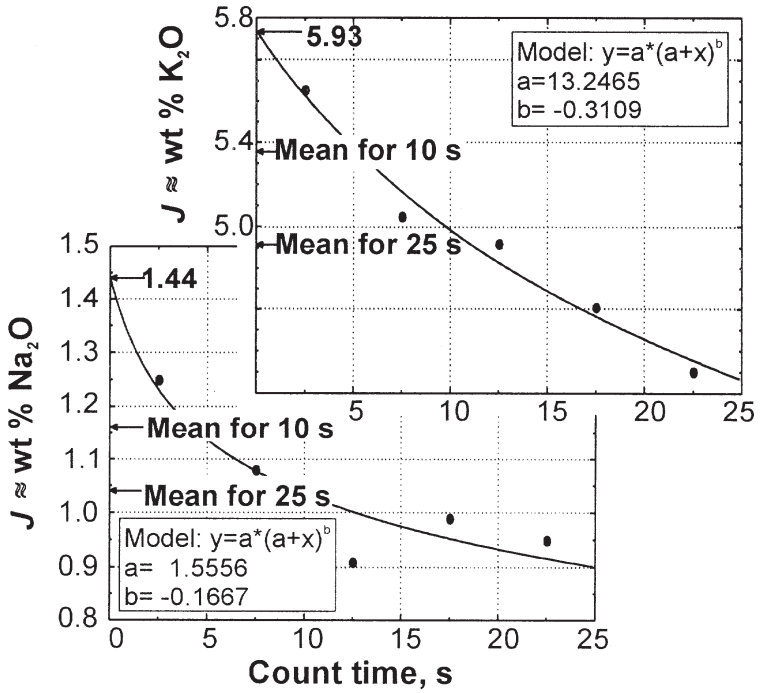

FIG. 6. The drop in intensity of the K and Na spectral lines ($J \approx$ wt% K_2O and Na_2O) with time, typical of electron-microprobe analysis of glassy melt inclusions. Values corresponding to the "zeroth" count time are believed to be the closest to true concentrations (sample Z78, MI q1).

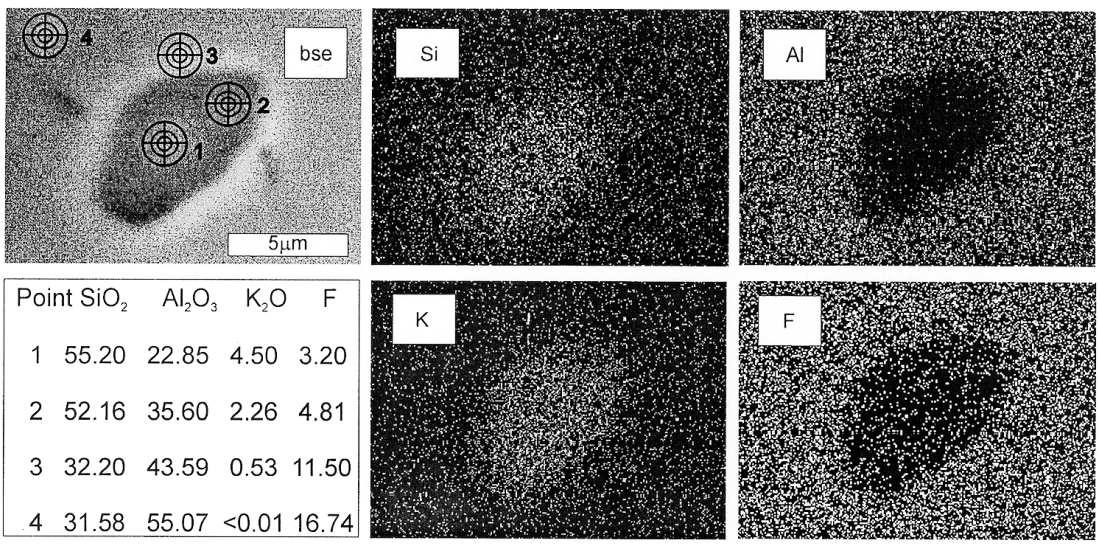

Point	SiO_2	Al_2O_3	K_2O	F
1	55.20	22.85	4.50	3.20
2	52.16	35.60	2.26	4.81
3	32.20	43.59	0.53	11.50
4	31.58	55.07	<0.01	16.74

FIG. 7. Back-scattered electron image and major-element maps (X-ray) of a topaz-hosted glassy melt inclusion from sample Sh57. Position and electron-beam diameter are shown to scale as target-like "points". The major-element concentrations (in wt%) listed on the lower left are obtained using SEM–EDS (points 1 to 3) and EPMA (point 4).

The pattern of data points in Figure 8 leads us to conclude that the compositions of topaz-hosted MI showing SiO_2 << 66 wt% and Al_2O_3 >> 16 wt% are not representative. Similarly, compositions of quartz-hosted MI showing SiO_2 >> 70 wt% are assumed to be unrepresentative of our case as well. The EPMA and SEM–EDS data that do not satisfy these constraints are excluded from further consideration except for analyses of MI–26 from sample A36 (No. 7–10 in Table 4), which are useful for interpretation of the following problem.

As can be seen from Table 4 (No. 1 and 2), two primary MI from different growth-zones of a single crystal of quartz show opposite K:Na ratios. This difference is unlikely to result from peculiarities of our analytical methods (EPMA and SEM–EDS), and may indicate that the melt composition changed with time during crystal formation. However, similarly different ratios that are associated with minor variations in Si and Al, and wide variation in the proportion of F, are typical for adjacent parts of the glassy MI–26 (compare No. 7, 8 and 9, 10 in Table 4). This MI was completely melted at 620°C and was held at 660°C for 4 h and then quenched. In this case, the observed difference cannot be explained by the excitement of the host mineral by the electron beam, and suggests a compositional heterogeneity of this glass, even though both low viscosity of the melt and small size of the inclusion (6 by 9 μm) would be expected to provide a homogeneous distribution of Na and K in melt before chilling. Therefore, we assume that compositional heterogeneity (as precrystallization state) may arise in low-viscosity melts during cooling. In view of the uncertainties discussed, the difference in K:Na ratio detected in the quartz-hosted MI cannot be interpreted unambiguously at present. Also, there still remains a question of whether the observed difference in $Na_2O + K_2O$ and hence ASI (aluminum saturation index) values between quartz-hosted and topaz-hosted inclusions (Table 4) is real or apparent.

As might appear at first sight, a rather significant deficit of the analytical total is balanced by the independently determined H_2O contents of MI (Fig. 4). It was shown above, however, that almost all H_2O dissolved in melt at the conditions of homogenization exsolves again upon chilling and forms a gas–liquid bubble (Fig. 2c), which is normally ground off in the course of preparation of inclusions for analysis. At the same time, the included melt may well be enriched in Li, undetectable *via* EPMA and SEM–EDS, although it is abundant in the Orlovka granites [790 to 1100 ppm: Zaraisky *et al*. (1997)]. This assumption seems to be all the more reasonable since Li, along with F, are components that will reduce melt viscosity to the greatest extent (Dingwell *et al*. 1996).

Inasmuch as there is no evidence that trapped melts differ significantly from a bulk melt in contents of major elements (see Discussion), the primary MI analyzed are believed to be a sample of the main-stage melts that are parental to the thin-banded and "transitional" granites (No. 1–3 in Table 4), whereas the secondary MI (No. 4–6 in Table 4) contain the late-stage, residual melts. Nevertheless, their compositions are similar in respect to major components, except for their Na_2O content. This difference may be artificial in view of the uncertainties inherent in our analyses.

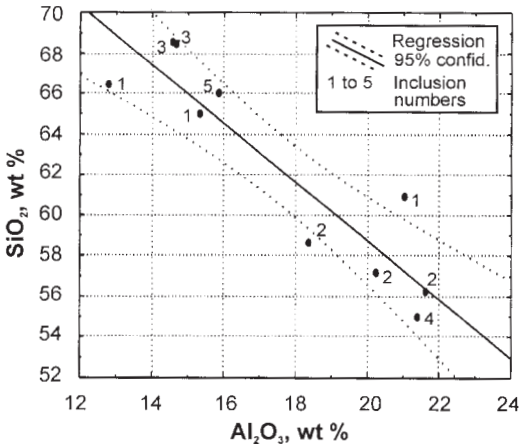

FIG. 8. Variation in EPMA estimations of SiO_2 and Al_2O_3 concentration in five cogenetic topaz-hosted MI from sample Sh57, attributed to a variable extent of host-mineral excitement. All the inclusions labeled 1–5 are confined to a single healed microfracture, some of them are analyzed at two or three points (see text).

As noted above, the unusually low viscosity of the melt in the inclusions studied raises a question: is it an aluminosilicate or aluminofluoride melt? The data shown in Table 4 prove unambiguously that the MI contain aluminosilicate melt, although distinctly depleted in SiO_2 and $Na_2O + K_2O$ and enriched in F as compared to the Orlovka Li–F granite and pegmatite reported by Zaraisky *et al*. 1997 (No. 14-19, respectively in Table 4). At the same time, the melts are similar in composition to the residual melt in the system granite–H_2O–HF at 1 kbar, 750 and 700°C (No. 12 and 13 in Table 4, Kovalenko 1979) and to MI in quartz from the high-F, high-P granitic pegmatite (No. 11 in Table 4, an average of 19 analyses, Webster *et al*. 1997). From this reasoning, we infer that: (1) owing to small sizes of the inclusions and the impossibility to defocus the electron beam, both EPMA and SEM–EDS underestimate the level of alkalis, especially Na, and (2) both the banded and massive granites studied in this work crystallized from melts similar in composition to residual melt in the F-rich hydrous granite system.

DISCUSSION

As follows from the above, both the massive and banded granites making up the sheet-like body in the

Orlovka cupola crystallized from H_2O- and fluorine-rich, low-viscosity melts containing a quantity of CO_2 in addition to H_2O. Although these granites suffered postmagmatic alteration, their textures formed at a magmatic stage, which suggests that the textural diversity results from the peculiar conditions of magma crystallization at different levels of the intrusion.

Conditions of cooling as a factor determining textural diversity of the rocks

It is a special feature of the banded granites occurring at the uppermost level of the pluton that fan-like and axiolitic aggregates of crystals are widespread, and the evidence for unidirectional crystal growth is pronounced. Also, zoning of both the groundmass quartz grains (Fig. 2g) and quartz megacrysts (Figs. 2h, i, 3) is typical for the banded and aplitic ("transitional") granites, although it is uncommon in the lower-level Li–F granites. One of the possible reasons for the formation of zoned crystals and banded rocks would be the wide fluctuations in pressure, which is a more variable parameter than temperature in a plutonic environment. In our case, however, the lack of detectable variation in densities and compositions of the MFI confined to different growth-zones in a multiply-zoned crystal argues against a wide fluctuation in pressure throughout the period of formation of a single crystal. Also, we show that the observed change in composition of the fluid exsolved from the melt throughout the degassing period is consistent with isobaric crystallization of parental magma (Fig. 5).

On the other hand, the textural features described are considered to be inherent to magmatic rocks crystallized from undercooled, and thus supersaturated, liquid in the presence of a significant temperature-gradient, where

TABLE 4. SELECTED RESULTS OF EPMA AND SEM-EDS ANALYSES OF MELT INCLUSIONS (MI) IN THE ORLOVKA Li–F-ENRICHED GRANITE, TANSBAIKAL, RUSSIA, AND BULK COMPOSITION OF THE SAMPLES SELECTED FOR STUDY

No.	Sample host mineral	MI origin and label	SiO_2	Al_2O_3	FeO	MnO	CaO	Na_2O	K_2O	F	Total	H_2O^a –O=2F	ASI
1	Z78, quartz	Prim., q2[b]	67.18	14.40	<0.52	0.39	0.05	6.00[c]	1.19[c]	n.a.	89.21	5.2 ± 0.8	1.3
2	- " -	Prim., q1	68.38	14.11	1.51	0.49	0.06	1.60[c]	5.98[c]	3.33	94.06	n.a.	1.6
3	Z19, topaz	Prim., t2	67.29	14.44	<0.04	<0.04	0.06	1.06[c]	2.74[c]	6.71	89.48	6.0 ± 0.7	3.1
4	Sh57, topaz	Sec., t1	66.39	12.81	0.41	0.31	0.29	0.34	4.50	7.18	89.21	9.9 ± 0.7	2.4
5	- " -	Sec., t3	68.59	14.56	0.04	0.31	0.73	0.84[c]	3.36[c]	1.05	89.04	- " -	2.9
6	- " -	Sec., t5	66.01	15.86	0.56	0.34	0.21	0.70[c]	2.95[c]	2.17	87.89	- " -	3.6
Mean of 4 to 6			67.00	14.41	0.34	0.32	0.41	0.53	3.60	3.46			
7	A36, topaz	Sec., 26	67.36	20.04	<0.06	<0.03	0.15	1.35	3.40	1.86	93.38	5.9 ± 0.5	3.4
8	- " -	Sec., 26	68.57	19.96	<0.06	<0.03	0.15	1.18	4.23	4.23	96.54	- " -	3.1
Mean of 7 and 8			67.96	20.00	0.15	1.26	3.82	3.04					
9	A36, topaz	Sec., 26	67.94	20.27	<0.06	<0.03	0.49	4.44	1.69	1.79	95.87	5.9 ± 0.5	2.2
10	- " -	Sec., 26	68.13	20.34	<0.06	<0.03	0.46	5.55	1.42	1.77	96.93	- " -	1.9
Mean of 9 and 10			68.04	20.30	0.48	5.00	1.56	1.78					
11	MI, pegmatite[d]		67.50	15.80	0.41	0.05	0.24	3.00	4.30	3.10	98.20[c]	1.2	1.6
12	RM, 750[f]		67.94	13.44	0.70	n.a.	n.a.	3.05	4.23	3.53	91.40	7.7	1.4
13	RM, 700[f]		64.88	14.39	0.85	n.a.	n.a.	3.72	4.41	4.17	90.66	7.3	1.3
14	A92, massive Li-F granite		71.20	17.00	0.78	0.08	0.08	6.30	4.00	0.18	99.54	n.a.	1.2
15	A36 - " -		73.30	15.80	0.40	0.08	0.11	4.89	4.50	1.40	99.89[g]	n.a.	1.1
16	Z73, two-mica granite		74.90	13.50	1.35	0.01	0.47	3.66	4.16	0.12	98.12[g]	n.a.	1.1
17	Z78, thin-banded granite		72.04	15.12	1.25	0.17	0.15	4.25	5.16	0.95	98.69[g]	n.a.	1.1
18	Z19, pegmatite		71.20	15.90	0.67	0.10	0.19	3.99	6.63	0.62	99.04[g]	n.a.	1.0
19	Sh57, pegmatite veinlet		76.60	13.40	0.65	0.08	0.37	1.15	5.37	2.28	98.96[g]	n.a.	1.4

MgO, P_2O_5, and Cl in melt inclusions studied are <0.06, <0.17, and ≤0.04 wt%, respectively; ASI: Aluminum Saturation Index: molar $[Al_2O_3/(Na_2O + K_2O + 0.5{\cdot}CaO)]$; n.a.: not analyzed.

[a] Estimations are based on volumetric and microthermometric data (Fig. 4), except for last three values. [b] Result from SEM-EDS analysis. [c] Values are recalculated using a procedure described in text and shown in Figure 6. [d] Melt inclusions in quartz from pegmatite (mean of 19 EPMA) from Erzgebirge P-rich Li–F-enriched granite (Webster *et al.* 1997). [e] Including 3.6% P_2O_5, 0.3% Li_2O, and 1.2% H_2O. [f] Residual melts in the system granite – H_2O – HF at 1 kbar, 750° and 700°C (Kovalenko 1979). [g] In addition, samples A36, Z73, Z78, Z19, and Sh57 contain <0.01, 0.25, 0.01, 0.01, and 0.01% TiO_2, respectively, <0.1, 0.3, <0.04, <0.04, and <0.04% MgO, respectively, <0.05, 0.07, 0.03, 0.01, and 0.01% P_2O_5, respectively.

the kinetics of mineral nucleation and growth play an important role in the formation of the rock's texture (*e.g.*, Kirkpatrick 1975, Petersen 1985, Swanson & Fenn 1986, Brandeis & Jaupart 1987). Under such conditions, the occurrence of multiple growth-zones may well be caused by the existence of so-called boundary layers, which accumulate components that are incompatible with quickly growing crystals, such that melt supersaturation and mass nucleation of the mineral(s) consuming incompatible elements occur. In the special case that topaz nucleation occurs just ahead of the surface of a quartz crystal, a depletion of the boundary-layer melt (BLM) in fluorine must suppress H_2O solubility (Kovalenko 1979, Holtz *et al*. 1993), which might give rise to the separation of fluid phase. This would explain why almost all topaz-rich growth-zones in quartz contain numerous MFI (Fig. 2f), as opposed to zones enriched in albite. In all likelihood, the drop in fluorine content of the BLM reduces not only the solubility of H_2O, but the solubility of tantalum as well. Evidence for such a drop is provided by the change in columbite–tantalite habit from acicular to dendritic just after the beginning of topaz nucleation (Fig. 2i). Such an inference agrees with the experimental data on solubilities of columbite–tantalite in granitic melts, which depend on fluorine content (Keppler 1993, Linnen & Keppler 1997). It must be emphasized that decrease in columbite–tantalite solubility, not an increase in Ta(Nb) concentration, provides the conditions for supersaturation in similar cases.

Clearly, the growth of crystals must be fast enough for the effect of a boundary layer to manifest itself, especially in the light of the data obtained on the very low viscosity of the trapped melt. In our case, the required rate of crystal growth was most likely attained as a result of undercooling of the melt at the upper level of the intrusion, where a temperature gradient was significant. Although boundary layers operate only on the scale of crystals, it seems highly probable that kinetic factors are responsible for the formation of thin-banded textures as well, since disequilibrium would work at any scale. This problem, of course, calls for further investigations; all factors considered, however, we believe that the textural features described are more likely to owe their origin to the undercooling of melt than to fluctuations in pressure or temperature.

Correspondence between the MI and bulk-melt compositions

In view of the evidence for influence of a boundary layer on formation of the Li–F granites, it is important to determine to what extent the boundary-layer melt differs in composition from the bulk melt. There is no way, in our case, in which this question can be clarified, except by revealing the difference in compositions of the MI hosted by quartz (only Si is compatible) and topaz (Si, Al, and F are compatible). Inasmuch as Si and Al possess the lowest diffusivity among the major elements in granitic melts (Johannes & Holtz 1996), their contents in quartz-hosted MI would be expected to differ from those in topaz-hosted MI if the trapped melt were in strong disequilibrium with a bulk melt.

Contrary to expectation, Si and Al contents of the MI hosted by these minerals are quite similar (No. 1, 2 and 3–6 in Table 4). This finding suggests that compositions of the MI studied are representative of the bulk melt, which was shown to be saturated in both quartz and topaz throughout crystallization of the Li–F granites (see Appendix A). Nevertheless, we believe that the composition of the BLM differentiated somewhat from that of the bulk melt during periods preceding the mass nucleation of topaz in front of growing quartz grains (light growth-zones in Figs. 2h, i). It is likely that the difference was not revealed by EPMA of the MI–1, 2 (Fig. 3, Table 4) because the latter formed when numerous topaz microcrystals had already nucleated, and supersaturation of the BLM in Al and F had been relieved. Although the distinction between compositions of the topaz-saturated bulk melt and supersaturated BLM remains unknown, it is assumed to be in the range of uncertainties inherent in the analytical procedure used in this investigation.

Saturation of Li,F-enriched melt in columbite–tantalite and Ta(Nb) content of magma

The key to understanding the role of magmatic processes in formation of the Ta mineralization lies in the finding that the melt was saturated in columbite–tantalite at certain stages of crystallization, as indicated by association of this mineral with MI in some growth zones of quartz from banded granites. Strictly speaking, the situation shown in Figure 2i does not provide an answer to the question as to whether only the boundary-layer melt or also the bulk melt was saturated in columbite–tantalite. In most cases, however, the opposite ends of a columnar crystal of columbite–tantalite are hosted by different minerals, microcline and quartz or microcline and albite (Fig. 2j), suggesting that at least a certain part of the former has crystallized from a bulk melt. Since such relationships are characteristic of the "transitional" aplitic granite, fine-grained parts of the banded granites, and fine-grained groundmass of the massive Li–F granite, we assume that these varieties crystallized from the melt saturated in columbite–tantalite.

As follows from the experimental results, the solubilities of manganocolumbite and manganotantalite in the iron-free granitic melts strongly depend on the molar ratio Al/(Na + K + 2Mn), temperature, and concentrations of H_2O and F (Keppler 1993, Linnen & Keppler 1997). In particular, at H_2O-saturated conditions (600°C, 2 kbar) and concentration of 0.05 wt% MnO in fluorine-free melt, 70 to 100 ppm Nb or 500 to 1400 ppm Ta are required for manganocolumbite and manganotantalite saturation, respectively.These values,

however, would decrease or increase with the increase of MnO (MnO + FeO) or F content, respectively.

The independent information on columbite–tantalite solubility in granitic melts comes from SIMS data on Ta content of MI in quartz from the pegmatite hosted by an unaltered F- and P-rich granite at the Ehrenfriedersdorf Sn–W mine, Erzgebirge, Germany (Webster *et al.* 1997). The presence of accessory columbite–tantalite in this pegmatite suggests that the pegmatite-forming melt was saturated relative to Ta and Nb at the final magmatic stage, at least locally. Taking into account that the Ta and Nb content of 12 MI ranges from 25 to 521 ppm and from 23 to 150 ppm, respectively, we assume that the highest of these values is characteristic of columbite-saturated melts and the lowest, of undersaturated ones. As a first approximation, the Ta content of a tantalite-saturated F-rich melt is expected to be about 200 ppm. If so, then the late-stage melt in the Orlovka cupola might also contain 200 ppm Ta, or 244 ppm Ta_2O_5, and hence only the whole-rock Ta_2O_5 content far in excess of 200 ppm requires an assumption that a quantity of Ta was added in such cases at the postmagmatic stage.

In reality, the average $Ta_2O_5(Nb_2O_5)$ content of the uppermost, ore-grade part of the Orlovka cupola (banded rocks included) and underlying massive Li–F granites is 180(120) ppm and 60(70) ppm, respectively (Zalashkova 1969). This is in agreement with the evidence that the melt became saturated in columbite–tantalite early in the crystallization at the upper level of the intrusion and late in the crystallization at the lower levels. Hence, the abundances of Ta_2O_5 and Nb_2O_5 determined in granites of the upper and lower levels are believed to be those of the parental magma. A subordinate contribution of the magma-derived fluids to the formation of the orebody can be explained in this case because enrichment of the exsolved fluid in CO_2 (Table 3, Fig. 5) entails a significant decrease of the fluid/melt partition coefficient for most lithophile elements, including Nb (Webster *et al.* 1989).

The reasons for occurrence of the most Ta(Nb)-enriched melt at the top of the intrusion

Taking into account that Ta and Nb are incompatible with major rock-forming minerals of granites (Rollinson 1993) and that the estimated viscosity of the melt was as low as ~50 Pa•s, the first possibility to be considered for an explanation of nonuniform Ta(Nb) distribution in the magmatic body is the enrichment of its apical parts in incompatible elements *via* crystal settling. To estimate the efficiency of this mechanism, model calculations were performed as applied to Ta, using the Stokes formula (1) with an assumption that crystals are spherical in shape, 1 to 10 mm in diameter, the crystals and melt densities are 2.6 and 2.25 g•cm^{-3}, respectively, the bulk partition coefficient for Ta is ~0.2 prior to beginning of columbite–tantalite crystallization, and the model melt viscosity is either 50 or 1000 Pa•s. Results of the calculations (Fig. 9) indicate that the settling of phenocrysts would be efficient even if the melt viscosity exceeded the value derived from the MI studies by more than an order of magnitude.

On the other hand, if the initial Ta content of the emplaced magma was ~60 ppm, a very efficient separation of phenocrysts from liquid would be required to obtain a melt with 180 ppm Ta. This may be illustrated using the equation for the Rayleigh-type fractionation:

$$C/C^* = F^{(k-1)} \quad (3)$$

where C and C^* are current and initial Ta content of the melt, respectively (180 and 60 ppm in this case), k is the bulk partition-coefficient for Ta (a value of 0.2 is accepted), and F is the mass fraction of melt, which varies from 1 to 0 as crystallization progresses. As can be seen in Figure 10, the settling of phenocrysts brought in with the emplaced magma (≤30 vol.% from the petrographic observation, which means $F \approx 0.7$) would be insufficient for the required threefold enrichment of melt in Ta (*a–b–c* in Fig. 10). Such enrichment would be attained only provided that 75% of the magma ($F = 0.25$) had crystallized and are devoid of crystals (*d–e–f* in Fig. 10) prior to the beginning of columbite–tantalite crystallization. This is highly improbable, because some textural features of the upper-level granites suggest that they crystallized in the presence of a significant temperature-gradient. Under such conditions, a relatively fast movement of the solidification front may suppress crystal settling.

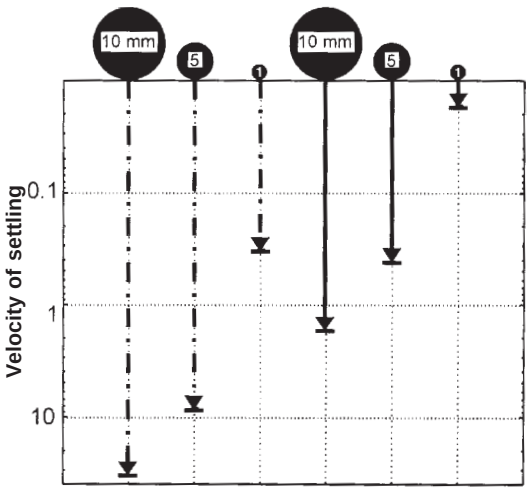

FIG. 9. Calculated velocity of settling (meters per day) of spherical phenocrysts 1 to 10 mm in diameter depending on accepted viscosity of the melt (dotted-dashed lines for 50 Pa•s, solid lines for 1000 Pa•s).

Irrespective of whether crystal settling occurs or not, a residual melt within the inner part of the intrusion must become enriched in Ta(Nb) until saturation when *F* falls below ~0.2, and this is the case that follows from the petrographic observations (see Appendix A). At $F < 0.2$, in the general case, a crystallizing magma contains a crystalline framework with a pore-space filled with residual melt. Removal of the latter requires either existence of a strong pressure-gradient or deformation of the framework, and is normally hampered in the granitic systems by the high viscosity of the melt. This restriction, however, is reduced in our case owing to the unusually low viscosity of the melt, which leaves room for a relatively easy migration and collection of the interframework residual melt inside cooling cracks within the crystalline carapace. Being almost devoid of crystals and somewhat undercooled, this melt could produce rocks exhibiting the textural features inherent to some granites from chilled zones of hypabyssal intrusions.

The latter scenario seems to be applicable to the formation of the Li–F granites for the following reasons. First, the banded granites form subhorizontal flattened lenses and steeply dipping dike-like bodies, much as the granophyric bodies, a conventional example of the segregated interstitial residual melt, occur in mafic sills (*e.g.*, Marsh 1996). Second, this scenario explains why the melt, located at the upper level of the magmatic body and undercooled, is enriched in Ta(Nb) to a maximum degree.

Conclusions

Banded granites occur at the upper, most intensely mineralized level of the Orlovka cupola, and hence might be expected to be a product of hydrothermal processes. However, these banded granites, as well as massive Li–F granites from lower levels, are shown to be formed from low-viscosity, CO_2-containing, H_2O- and F-rich aluminosilicate melt, similar in composition to residual melts in the system granite–H_2O–HF. Some textural features of the banded rocks suggest that their parental melt crystallized faster than the melt producing the massive granites owing to the existence of a temperature gradient, and this is assumed to be a prerequisite to the formation of the banded texture. The banded rocks exhibit petrographic evidence that their parental melt became tantalite-saturated during the early stages of crystallization and, consequently, was highly enriched in Ta(Nb). With regard to the results of model calculations, the location of the most evolved, Ta(Nb)-rich melt at the apical part of the magmatic body is likely to be caused by the removal of interstitial residual melt from the deeper part of the intrusion into the previously solidified crystalline carapace rather than by crystal settling.

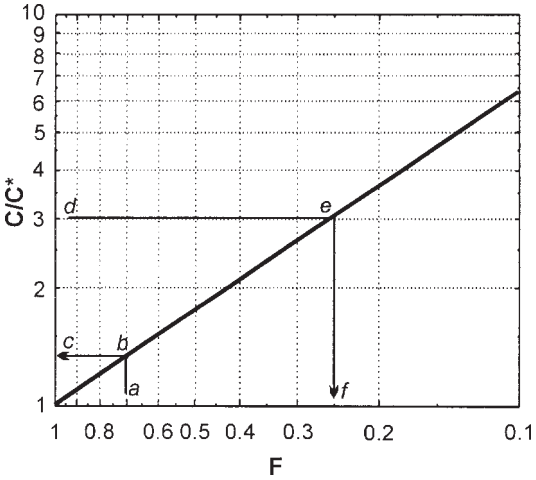

FIG. 10. Increase of Ta concentration in the melt (**C**) with respect to that in initial magma (**C***) as mass fraction of the melt (**F**) decreases from 1 to 0.1, provided that Rayleigh-type fractionation occurs (see text for explanation).

Acknowledgements

We thank T. Salova (IEM, Chernogolovka), whose experimental equipment was used, in part, to heat the melt inclusions under confining gas pressure. We appreciate assistance of S. Kanakin, N. Karmanov (GIN, Ulan-Ude), and M. Lapina (IGEM, Moscow) in EPMA and SEM–EDS studies as well as participation of L. Reyf in volumetry of melt inclusions and estimation of their H_2O content. Our special thanks to J.D. Webster (AMNH, New York) and R. Armstrong (NHM, London) for reading and discussing earlier versions of the manuscript and for improvement of the English text, and C. Stanley (NHM, London) and R. Thomas (GFZ, Potsdam) for stimulating criticism. Editorial suggestions and critical comments made by R.F. Martin, D.J. Kontak, W.D. Sinclair and an anonymous reviewer were very useful in preparation of the present text. This research was supported by the Russian Foundation of Base Research (RFBR grant 96–05–64057) and, in part, by the Deutsche Forschungsgemeinschaft (DFG) SE 594/7–1 and by the INTAS–93–1783 project. This is a contribution to the IGCP project 373 on "Ore-bearing granites of Eurasia".

References

AUBERT, G. (1969): Les coupoles granitiques de Montebras et d'Echassières (Massif Central Français) et la genèse de leurs minéralisations en étain, lithium, tungstène, et béryllium. *Bureau de Recherches Géologiques et Minières, Mém.* **46**.

BESKIN, S.M., GREBENNIKOV, A.M. & MATIAS, V.V. (1994): The Khangilay granite pluton and related Orlovka tantalum deposit, Transbaikalia. *Petrologiya* **2**, 68-87 (in Russ.).

BEUS, A.A., SEVEROV, E.A., SITNIN, A.A. & SUBBOTIN, K.D. (1962): *Albitized and Greisenized Granites* (*apogranites*). Akad. Nauk SSSR, Moscow, Russia (in Russ.).

BRANDEIS, G. & JAUPART, C. (1987): The kinetics of nucleation and crystal growth and scaling laws for magmatic crystallization. *Contrib. Mineral. Petrol.* **96**, 24-34.

_____, _____& ALLÈGRE, C.J. (1984): Nucleation, crystal growth and the thermal regime of cooling magmas. *J. Geophys. Res.* **89**, 10,161-10,177.

BROWN, P.E. (1989): FLINCOR: a microcomputer program for the reduction and investigation of fluid-inclusion data. *Am. Mineral.* **74**, 1390-1393.

BURNHAM, C.W. (1979): Magmas and hydrothermal fluids. *In* Geochemistry of Hydrothermal Ore Deposits (H.L. Barnes, ed.). John Wiley & Sons, New York, N.Y. (71-136).

CARTEN, R.B., GERAGHTY, E.P., WALKER, B.M. & SHANNON, J.R. (1988): Cyclic development of igneous features and their relationship to high-temperature hydrothermal features in the Henderson porphyry molybdenum deposit, Colorado. *Econ. Geol.* **83**, 266-296.

DINGWELL, D.B., HESS, K.-U. & KNOCHE, R. (1996): Granite and granitic pegmatite melts: volumes and viscosities. *Trans. R. Soc. Edinburgh, Earth Sci.* **87**, 65-72.

FENN, P.M. (1977): The nucleation and growth of alkali feldspars from hydrous melts. *Can. Mineral.* **15**, 135-161.

GLJUK, D.S. & ANFILOGOV, V.N. (1975): Peculiarities of phase relations in acid silicate systems with fluorine and water. *In* Formation of Granites and Volatiles (S.N. Ivanov, ed.). Proc. Inst. Geol. and Geochem., Akad. Nauk SSSR, Uralian Sci. Centre (Sverdlovsk) **120**, 38-46 (in Russ.).

HOLTZ, F., DINGWELL, D.B. & BEHRENS, H. (1993): Effects of F, B_2O_3 and P_2O_5 on the solubility of water in haplogranite melts compared to natural silicate melts. *Contrib. Mineral. Petrol.* **113**, 492- 501.

HU, SHUOXI, SUN, MINGZHI, YAN, ZHENGFU, XU, JINFANG, GAO, XIAOYUN & YE, YING (1984): An important metallogenetic model for W, Sn and rare granitophile element ore deposits related to metasomatically altered granites. *In* Proceedings of International Symposium on Geology of Granites and their Metallogenetic Relations. University Nanjing, Nanjing, People's Republic of China (519-537).

JAUPART, C. & BRANDEIS, G. (1986): The stagnant bottom layer of convecting magma chambers. *Earth Planet. Sci. Lett.* **80**, 183-199.

JOHANNES, W. & HOLTZ, F. (1996): *Petrogenesis and Experimental Petrology of Granitic Rocks*. Springer-Verlag, Berlin, Germany.

KEPPLER, H. (1993): Influence of fluorine on the enrichment of high-field-strength trace elements in granitic rocks. *Contrib. Mineral. Petrol.* **114**, 479-488.

KIRKPATRICK, R.J. (1975): Crystal growth from the melt: a review. *Am. Mineral.* **60**, 798-814.

KOVAL, P.V. (1975): *Petrology and Geochemistry of Albitized Granites.* Nauka, Novosibirsk, Russia (in Russ.).

KOVALENKO, N.I. (1979): *Experimental Investigation of the Formation of Rare-Metal Lithium–Fluorite Granites*. Nauka, Moscow, Russia (in Russ.).

KUTATELADZE, S.S. (1990): *Heat Transmission and Hydrodynamic Resistance: a Handbook.* Energoatomizdat, Moscow, Russia (in Russ.).

LEMMLEIN, G.G. & KLEVTSOV, P.V. (1956): Effect of concentration upon the homogenization temperature of the systems consisting of salt aqueous solutions. *Zap. Vses. Mineral. Obshchest.* **85**, 310-320 (in Russ.).

_____, KLIYA, M.O. & OSTROVSKY, I.A. (1962): On conditions of the formation of pegmatite minerals as evidenced from studies of primary inclusions in topaz. *Dokl. Akad. Nauk SSSR* **142**, 81-83 (in Russ.).

LINNEN, R.L. & KEPPLER, H. (1997): Columbite solubility in granitic melts: consequences for the enrichment and fractionation of Nb and Ta in the Earth's crust. *Contrib. Mineral. Petrol.* **128**, 213- 227.

LONDON, D. (1998): Experimental simulation of pegmatite texture. *Int. Mineral. Assoc., 17th General Meet.* (*Toronto*), *Abstr. Vol.*, A144.

_____, HERVIG, R.L., & MORGAN, G.B., VI (1988): Melt–vapor solubilities and elemental partitioning in peraluminous granite – pegmatite systems: experimental results with Macusani glass at 200 MPa. *Contrib. Mineral. Petrol.* **99**, 360-373.

LOWENSTERN, J.B. & SINCLAIR, W.D. (1996): Exsolved magmatic fluid and its role in the formation of comb-layered quartz at the Cretaceous Logtung W–Mo deposit, Yukon Territory, Canada. *Trans. R. Soc. Edinburgh, Earth Sci.* **87**, 291-303.

MARSH, B.D. (1996): Solidification fronts and magmatic evolution. *Mineral. Mag.* **60**, 5-40.

NAUMOV, V.B. (1979): Determination of concentration and pressure of volatiles in magmas from inclusions in minerals. *Geochem. Int.* **16**, 33-40.

NEGREY, E.V., FAM TYK SUAN, GRAMENITSKY, E.N. & REYF, F.G. (1989): Orbicular granites of the Kent pluton (central Kazakhstan) and problems related to their origin *Izv. Akad. Nauk SSSR, Ser. Geol.* **3**, 17-30 (in Russ.).

_____, ZHURAVLEV, A.Z., KOVALENKO, V.I., YARMOLUK, V.V. & SHATAGIN, K.N. (1995): Isotopic (Rb–Sr, ^{18}O) stud-

ies of tantalum-bearing lithium–fluorine granite. *Dokl. Akad. Nauk* **342**, 522-525 (in Russ.).

PERSIKOV, E.S. (1984): *Viscosity of Magmatic Melts*. Nauka, Moscow, Russia (in Russ.).

PETERSEN, J.S. (1985): Columnar-dendritic feldspars in the lardalite intrusion, Oslo region, Norway. I. Implications for unilateral solidification of a stagnant boundary layer. *J. Petrol.* **26**, 223-252.

POTAP'EV, V.V. (1971): Internal structure and ore mineralization of the Mesozoic granite massifs. *In* Granitoid Massifs of Siberia and Ore Mineralization (F.N.Shakhov, ed.). Nauka, Novosibirsk, Russia (5-90; in Russ.).

POVILAITIS, M.M. (1961): About rhythmic zonality of some granitic bodies. *Izv. Akad. Nauk SSSR, Ser. Geol.* **2**, 35-50 (in Russ.).

_____ (1990): *Rhythmically Layered Granite Intrusions and Metallization.* Nauka, Moscow, Russia (in Russ.).

RAIMBAULT, L., CUNEY, M., AZENCOTT, C., DUTHOU, J.L. & JORON, J.L. (1995): Geochemical evidence for a multistage magmatic genesis of Ta–Sn–Li mineralization in the granite at Beauvoir, French massif central. *Econ. Geol.* **90**, 548-576.

REYF, F.G. (1973): Inclusions of melt in quartz of postorogenic granites of central Buryatiya and the pressures and temperatures accompanying their formation. *Dokl. Acad. Sci. USSR* **213**, 172-174.

_____ (1990): *Ore-Forming Potential of Granites and Conditions for its Realization*. Nauka, Moscow, Russia (in Russ.).

_____ (1997): Direct evolution of W-rich brines from crystallizing melt within the Mariktikan granite pluton, west Transbaikalia. *Mineral. Deposita* **32**, 475-490.

_____, SERYH, V.I. & KANAKIN, S.V. (1989): Conditions of formation of the Akchatau topaz-bearing biotite–albite granites. *Dokl. Akad. Nauk SSSR* **306**, 953-956 (in Russ.).

ROLLINSON, H.R. (1993): *Using Geochemical Data: Evaluation, Presentation, Interpretation.* Longman Group Ltd., Essex, U.K.

RYABCHIKOV, I.D. (1975): *Thermodynamics of Fluid Phase of Granitic Magmas*. Nauka, Moscow, Russia (in Russ.).

SELTMANN, R., TAYLOR, B., AKSYUK, A.M., FEDKIN, A.V., REYF, F.G., SHATOV, V.V. & ZARAISKY, G.P. (1998): Line rock formation in the Orlovka and Etyka tantalum deposits, eastern Transbaikalia. *Int. Mineral. Assoc., 17th General Meet.* (*Toronto*), *Abstr. Vol.*, A148.

SHANNON, J.R., WALKER, B.M., CARTEN, R.B. & GERAGHTY, E.P. (1982): Unidirectional solidification textures and their significance in determining relative ages of intrusions at the Henderson mine, Colorado. *Geology* **10**, 293-297.

SHARAPOV, V.N. & GOLUBEV, V.S. (1976): *The Dynamics of Interaction between Magma and Rocks.* Nauka, Novosibirsk, Russia (in Russ.).

STELMACHONOK, K.Z. & KANAKIN, S.V. (1992): Dependence of melt inclusion mineralogy on water content and host mineral composition. *In* Thermobarogeochemistry of Geological Processes. VIII Symposium on Thermobarogeochemistry. Aleksandrov, Russia (abstr.; in Russ.).

STUDENT, J.J. & BODNAR, R.J. (1996): Melt inclusion microthermometry: petrologic constraints from the H_2O-saturated haplogranite system. *Petrology* **4**, 291-306.

SWANSON, S.E. & FENN, P.M. (1986): Quartz crystallization in igneous rocks. *Am. Mineral.* **71**, 331- 342.

THOMAS, R. (1994): Estimation of the viscosity and the water content of silicate melts from melt inclusion data. *Eur. J. Mineral.* **6**, 511-535.

_____ & KLEMM, W. (1997): Microthermometric study of silicate melt inclusions in Variscan granites from SE Germany: volatile contents and entrapment conditions. *J. Petrol.* **38**, 1753-1765.

_____, RHEDE, D. & TRUMBULL, R.B. (1996): Microthermometry of volatile-rich silicate melt inclusions in granitic rocks. *Z. Geol. Wiss.* **24**, 507-528.

WEBBER, K.L., FALSTER, A.U., SIMMONS, W.B. & FOORD, E.E. (1997): The role of diffusion-controlled oscillatory nucleation in the formation of line rock in pegmatite–aplite dikes. *J. Petrol.* **38**, 1777-1791.

WEBSTER, J.D. (1990): Partitioning of F between H_2O and CO_2 fluids and topaz rhyolite melt. *Contrib. Mineral. Petrol.* **104**, 424-438.

_____, HOLLOWAY J.R. & HERVIG R.L. (1989): Partitioning of lithophile trace elements between H_2O and H_2O + CO_2 fluids and topaz rhyolite melt. *Econ. Geol.* **84**, 116-133.

_____, THOMAS, R., RHEDE, D., FÖRSTER, H.-J. & SELTMANN, R. (1997): Melt inclusions in quartz from an evolved peraluminous pegmatite: geochemical evidence for strong tin enrichment in fluorine-rich and phosphorus-rich residual liquids. *Geochim. Cosmochim. Acta* **61**, 2589-2604.

WHITE, W.H., BOOKSTROM, A.A., KAMILLI, R.J., GANSTER, M.W., SMITH, R.P., RANTA, D.E. & STEININGER, R.C. (1981): Character and origin of Climax-type molybdenum deposits. *Econ. Geol., Seventy-Fifth Anniv. Vol.*, 270-316.

XIA, HONGYUAN & LIANG, SHUYI (1985): The evolutionary characteristics and mineralization of the W-bearing and Ta,Nb-bearing granites in South China. *In* The Crust – the Significance of Granite- Gneisses in the Lithosphere. Theophrastus, Athens, Greece (571-585).

YEROKHIN, A.M. (1993): A new method of determining CO_2 density and solution concentration in H_2O–CO_2–NaCl inclusions from the gas-hydrate melting point. *Geochem. Int.* **30**, 107-129.

YIN, LIN, POLLARD, P.J., HU, SHOUXI & TAYLOR, R.G. (1995): Geologic and geochemical characteristics of Yichun Ta–Nb–Li deposit, Jiangxi province, South China. *Econ. Geol.* **90**, 577-585.

ZALASHKOVA, N.E. (1969): A zoning of metasomatically altered tantalum-bearing granites (apogranites). *In* Mineralogical-Geochemical and Genetic Features of Rare-Metal Apogranite (K.D.Subbotin, ed.). Nauka, Moscow, Russia (5-29; in Russ.).

ZARAISKY, G.P., SELTMANN, R., SHATOV, V.V., AKSYUK, A.M., SHAPOVALOV, YU.B. & CHEVYCHELOV, V.YU. (1997): Petrography and geochemistry of Li–F granites and pegmatite–aplite banded rocks from the Orlovka and Etyka tantalum deposits in Eastern Transbaikalia, Russia. *In* Mineral Deposits: Research and Exploration. Where Do they Meet? (H. Papunen, ed.). Balkema, Rotterdam, The Netherlands (695-698).

Received January 4, 1999, revised manuscript accepted May 11, 2000.

APPENDIX A. KEY SAMPLES

Samples Z8, Z41 and Z73 consist of porphyritic two-mica granite in which quartz, microcline, and albite- oligoclase form both the phenocrysts (6 to 10 mm in size) and groundmass (≤3 mm). Partial replacement of biotite and microcline by muscovite and albite, respectively, is common, as if these rocks were a product of hydrothermal alteration of a biotite granite. However, both the phenocrystic and groundmass quartz grains contain microcrystals of biotite and muscovite 0.01–0.05 mm in size, and these are typically confined to separate or concentric growth-zones along with magmatic zircon and fluorapatite (No. 6–8 and 12 in Table 2). Hence, at least part of the rock-forming muscovite is thought to have crystallized from a melt. The same is true of small (≤10 μm) globular particles of fluorite (No. 16 and 17 in Table 2).

Sample A36 represents the massive, unbanded variety of Li–F granite ("albitized granites enriched in muscovite and Li mica" in Fig. 1). It consists of fine-grained (≤1 mm) quartz – microcline – albite aggregates containing up to 30 vol.% of coarser (3–4 mm) subhedral phenocrysts of quartz and, to a lesser extent, topaz, Li-enriched mica, and rarely microcline. Quartz and topaz contain albite as micro-inclusions (10–60 μm); biotite micro-inclusions are not observed. A few of the quartz phenocrysts contain micro-inclusions of topaz and, rarely, elongate columbite–tantalite within their marginal zone. In contrast, similar inclusions are rather common in the groundmass quartz, suggesting that columbite–tantalite crystallized later, during formation of the fine-grained groundmass.

Sample Z19 represents a pegmatite–aplite variety of the Li–F granite (a transitional type between massive and thin-banded granites). The aplitic part of this sample (and these rocks) is a fine-grained (0.3 to 0.6 mm) aggregate of quartz, microcline, albite (25–30 vol.% each), Li-enriched mica (5–7 vol.%), and topaz (2–5 vol.%) with minor acicular and columnar columbite–tantalite microcrystals (Fig. 2j). Smaller (20–50 μm) albite microcrystals in topaz, as well as albite and topaz in quartz, are typical of this rock. Some quartz grains contain rare round micro-inclusions of fluorite (No. 18 in Table 2). The presence of zoned quartz grains is a special feature of the aplitic granite. The core of such grains is filled with very small (1–4 μm) topaz and fluid inclusions, whereas the outer zone is free or almost free of them (Fig. 2g). Unzoned quartz grains either with or without the inclusions also occur as separate grains. In this fine-grained matrix, columnar or wedge-like, centimeter-sized megacrysts of "amazonite", quartz and, rarely, topaz occasionally form fan-shaped aggregates which grew in one direction (downward, at outcrops). The pegmatitic part of the sample forms a layer 7–8 cm thick that is composed of the described megacrysts (60 to 80 vol.%), which are hosted in a fine-grained matrix that is similar to the adjacent aplitic layer.

Sample Z78 is a thin-banded rock that consists of intermittent layers 2 to 8 mm thick composed of either fine-grained (0.15 to 0.3 mm) quartz–albite aggregates with minor microcline and topaz or medium- to coarse-grained aggregates of quartz, microcline ("amazonite"), and Li-rich mica with subordinate albite, topaz, and scarce beryl. Columnar columbite–tantalite microcrystals (≤10 μm thick, ≤150 μm long) are common in all layers.

Many large (≤6 mm) quartz subhedra in coarse-grained layers are zoned and show the growth vectors to be unidirectional irrespective of the layer to which the crystal belongs. The growth zones differ from each other in the amount of crystalline micro-inclusions and their composition. Some of these zones are enriched in an unidentified hair-like mineral or in tabular albite

microcrystals (No. 11 in Table 2, Fig. 3). Also, micro-inclusions of light-colored mica that are enriched in F, Fe, Mn and depleted in Mg (zinnwaldite?, No. 9 and 10 in Table 2) form marginal zones in some quartz crystals. However, growth zones filled with ≤15 μm-sized topaz microcrystals (No. 13–15 in Table 2, Fig. 2h) and fluid inclusions (Fig. 2f) are the most common and sharply defined. Many such zones contain acicular or dendritic columbite–tantalite crystals (Figs. 2i, 3), and some are free of fluid inclusions. Taking into account the fact that only one type of mineral micro-inclusion predominates in each zone, and that its size is more than an order of magnitude less than that of mineral grains in adjacent fine-grained layer(s), the micro-inclusions are considered to represent minerals cocrystallizing with a host rather than relics of a fine-grained rock replaced by the quartz porphyroblast.

Sample Sh57 consists of two parts: thin-banded Li–F granite and a pegmatite veinlet 1.5 cm thick cutting the layers at a right angle, and hence, representing one of the youngest derivatives of the Li–F granite. The thin-banded part is similar to that from sample Z78; however, it is poorer in columbite–tantalite and devoid of beryl. The pegmatite veinlet is composed of coarse-grained (5 to 8 mm) aggregates of quartz and "amazonite" with subordinate and finer grained (2 to 4 mm) albite, topaz, and Li mica. The veinlet selvages are enriched in quartz and contain scarce topaz and columnar crystals of "amazonite" oriented perpendicular to the contacts. A similar orientation also is typical for radiate-acicular aggregates of columbite–tantalite. A lack of zonality and growth zones filled with topaz and fluid micro-inclusions differentiate the pegmatite quartz from that belonging to the thin-banded part of this sample.

APPENDIX B. INSTRUMENTATION AND TECHNIQUES

Microthermometry

A heating stage with a silicon carbide heating element was used along with a Pt/Pt–Rh thermocouple calibrated using known melting points of seven chemically pure materials and two FI synthesized at controlled temperature and pressure. The power-law best fit of these data yields standard error of estimates ±5.1°C in the range from 100° to 1100°C and ±1.7°C in the range from 150° to 350°C.

When using the heating stage, a temperature cycling in the range from 100 to 350°C was carried out to determine the temperature of homogenization of fluid constituents of all preselected MI. Then temperature was raised to 580–600°C in 30–40 min and was maintained constant over 1.5–2 hours. Further heating was stepwice, with 1.5–2 hr isothermal exposure after each step and temperature increment of 50° to 20°C depending upon attained degree of melting of crystalline phases.

Heating of MI under confining argon pressure using a high-pressure vessel with internal heater was conducted at the Institute of Experimental Mineralogy (IEM RAS), Chernogolovka. Upon heating, pressure was raised up to 5 kbar along the isochore chosen in accordance with averaged density of a fluid constituent of the MI and then held constant during 8 to 20 h at a preselected temperature. The reverse path was used when cooling.

The cooling stage is equipped with a copper-constantan thermocouple calibrated with inclusions of pure CO_2 (determined using Raman spectroscopy) homogenized in liquid at different temperatures (determined using a mercury thermometer with accuracy of ±0.1°C) and with solutions of known eutectic temperatures introduced into elongate cavities, abundant in some technical quartz glasses. The deviation of the data points from the exponential best fit does not exceed ±0.2°C in the range from +30° to –56°C.

Electron-microprobe analysis

Crystallized and glassed MI as well as mineral microcrystals are analyzed at the Geological Institute (GIN SB RAS), Ulan-Ude, using the analyzer MAR–3 produced by the Krasnogorsky Mechanical Plant. The samples were analyzed at 20 kV, 40 nA beam current using a spot size of 4 μm for glass and 2 to 4 μm for crystals, 10 s count time for crystals and some glassy inclusions. Most of the latter were analyzed using 25 s total count time with data collected every 5 s. An attempt to decrease beam current was not successful, since it resulted in significant increase of random error. Several glassy MI were analyzed at the IGEM RAS, Moscow, using a scanning electron microscope JSM 5300 with a LINK ISIS energy-dispersion spectrometer at 25 kV acceleration voltage, approximately 1 nA current, about 2 μm spot size, 60 s count time, with readings taken every 12 s.

Determination of the H_2O content in melt inclusions ($_{Wcmi}$)

The determination is based on the following concepts that were originally described by Naumov (1979) and then refined by Reyf (1990).

(1) In the isochoric hydrous system of low to moderate salinity, the homogenization temperature (T_h) is unequivocally determined by the "filling coefficient" $F = V_{liq}/(V_{liq} + V_{gas})$ where V_{liq} and V_{gas} are the volumes of liquid and gaseous phases, respectively, at 20°C (*e.g.*,

plot of T_h *versus* F by Lemmlein & Klevtsov 1956). Hence, the volume of fluid constituent of a MI, $V_{fl} = V_{gas}/(1 - F)$, may be calculated provided that its salinity (C_{sal}) and T_h are determined thermometrically and the volume of the gas bubble at 20°C is measured with sufficient accuracy, using the Fedorov universal stage. Assuming that the mass of H_2O within a gas bubble at 20°C is negligible, the bulk density of the fluid is accepted to be equal to the F value, and the mass of hydrous solution WM_{fl} is equal to $F \bullet V_{fl}$. If muscovite is present among crystalline phases, its H_2O content must be accounted for: $WM_{ms} = V_{ms} \bullet d_{ms} \bullet 0.04 = 0.114 \bullet V_{ms}$, where V_{ms} and d_{ms} are measured volume and mean density (2.85 g•cm^{-3}) of muscovite; the weight proportion of 0.04 is typical H_2O content of muscovite. Thus, the total mass of H_2O in a melt inclusion WM_{mi} is equal to $WM_{fl} + WM_{ms}$.

(2) The MI volume measured prior to heating (V_{mi}*) is only a part of the total volume of inclusion (V_{mi}); it is indeterminable at such conditions because the material identical to a host mineral precipitates at the cavity walls and inherits its optical orientation. Upon heating, however, the precipitated material goes into the melt, resulting in the increase of the visible size of MI (*e.g.*, Figs. 2g, h, i in Reyf 1997). At the point of full homogenization, the measured ratio V_{mi}/V_{mi}* for the quartz-hosted MI varies from 1.6 to 1.8, depending on which mineral(s) (feldspars or muscovite) predominate among crystalline phases. Assuming that the mean density of a MI crystalline constituent is equal to that of granites (2.7 g•cm^{-3}), its mass is accepted to be $CM_{mi} = 2.7(V_{mi} - V_{fl})$. With the proviso that all volumetric data are presented in percent relative to V_{mi}*, the calculated H_2O content of melt inclusion (in wt%) is:

$$WC_{mi} = 100 \bullet WM_{mi} / (WM_{mi} + CM_{mi})$$

The measurement of parameters used in calculations (V_{gas}, V_{mi}*, V_{mus}, V_{mi}, T_h and C_{sal}) is associated with random errors that affect the accuracy of estimation of the WC_{mi} value. The measurements of V_{gas} and V_{mi}* in 75 MI that are 4 to 25 μm in diameter were performed independently by two investigators; the double measurements differ from the mean by less than 15% in 92% of the cases (less than 10% in 88% of the cases). The uncertainties in determination of the values of T_h (within the range from 150% to 350°C) and C_{sal} are found to be ≤3°C and ≤3 wt% NaCl equivalent, respectively. Assuming that measurements of the V_{gas}, V_{mus}, V_{mi}, T_h and C_{sal} are associated with maximum random errors of 15%, 20%, 20%, 5°, and 50% respectively, these errors are calculated to result in an overestimation or underestimation of the WC_{mi} value (within the range from 2 to 10 wt% H_2O) by 3 to 15% relative each, the contribution of the volumetric errors being the greatest. If errors in measurement of the listed parameters are of the same sign, the effect of some of them upon WC_{mi} is opposite in sign and, hence, the total error is believed to be generally of about 15% relative. In a special case, in which the effects of all errors in measurements are of the same sign, the additive (total) error in determination of the WC_{mi} value would attain 40% relative. However, such a case is unlikely to be common; in addition, it can be identified provided that several cogenetic inclusions are measured.